POLITECNICO DI MILANO

Scuola di Ingegneria Industriale e dell'Informazione

CORSO DI LAUREA MAGISTRALE IN INGEGNERIA AERONAUTICA

The Tandem Wing: Theory, Experiments, and Practical Realisations

Relatore:
Prof. Lorenzo Trainelli

Candidato:
Angelo Minardo
matr. 725266

Anno accademico 2013/2014

Contents

List of Figures

Part I

Introduction

Chapter 1

Tandem Configuration

The advantages of a tandem wing configuration have been backed since the early days of manned flight. From the Prandtl biplane theory to Navier Stokes numerical simulation, all works centred on the tandem wing configuration achieve similar if not identical conclusions. Such configuration is advantageous but there is no single design criteria to be followed, in depth analysis must be made for each single configuration depending on mission specs, wanted sizes and weights, and needed design features.

1.1 Objective

The objective of this paper is to narrate the history, describe the different designs, analyse past scientific work, and introduce a mathematical model set to simulate the flight characteristics, of the tandem configuration.

1.2 Configuration Design

The study of the tandem wing dates its roots to the very first manned flight, as the Wright Flyer in itself was a canard configuration aircraft. Ever since the study of canard, biplane, and tandem wings closely followed one another.

According to Prandtl, the lifting system with minimum induced drag is a proper box-like wing (named "Best Wing System"), in which the following conditions are satisfied: same lift distribution and same total lift on each of the horizontal wings and butterfly shaped lift distribution on the vertical tip wings. When these conditions of minimum occur, the velocity induced by the free vortices is constant along the two horizontal wings and identically zero on the vertical side wings (these are the Munk's conditions for minimum induced drag). The efficiency depends on the gap between the horizontal wings and, in particular, the induced drag decreases for increasing non-dimensional gap (that is: gap-to-span-ratio).

Prandtl's work, and Munk's conditions were then applied to canard and tandem aircraft by Laitone, while significant presentation of the configuration's character-

Figure 1.1: Scaled Composites Proteus.

istics was edited in an article published in Flight magazine April 1944. It's findings and conclusions are hereby presented.

1.2.1 Definitions

- **Tandem Wing Configuration**

  A tandem wing aircraft presents two independent lift generating wings (thus eliminating the need for a conventional horizontal plane on the aircraft's tail). Both wings have comparable aspect ratios and are typically set on two different planes separated both vertically and horizontally (Fig. 1.1).

- **Delanne Wing Configuration**

  Tandem wing configuration, where the rearmost wing tends to be smaller in size, much like an oversized tailplane. Named after Maurice Delanne, a French designer of tandem wing aircraft (Fig 1.2).

- **Canard Configuration**

  Configuration which presents a relatively small forewing or foreplane placed ahead of the main wing. Much like the tandem wing configuration, this would be separated both vertically and horizontally from the much larger main wing, and could completely eliminate the need for a conventional horizontal plane on the aircraft's tail (Fig. 1.3).

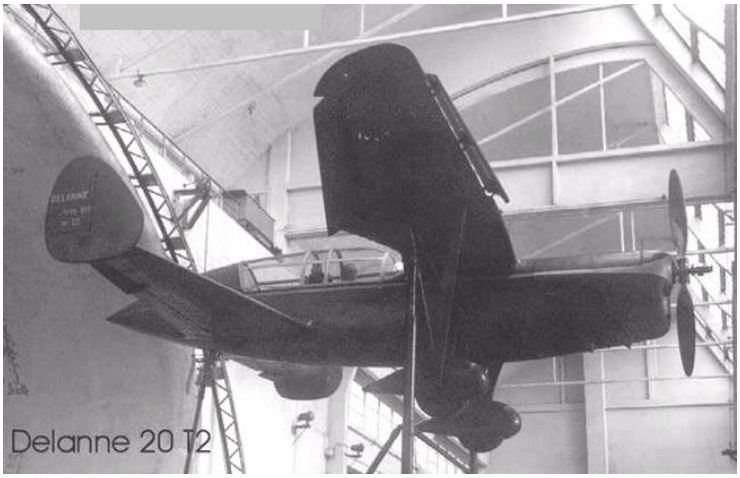

Figure 1.2: Delanne $20\ T2$.

Figure 1.3: Piaggio $P180$ Avanti, designed in part by Jan Roskam.

Figure 1.4: Secret design UAV for the Chinese People's Liberation Army Air Force, the Guizhou Soar Dragon.

- **Closed Wing Configuration**

  The closed wing configuration is a broad selection of unconventional aircraft configurations, which include; joined wing, box wing, and annular wing configuration. These configurations may be compared with the tandem wing configuration, when they present a horizontal separation of the upper and lower wing (example of a joined wing configuration Fig. 1.4).

- **Stagger** (St)

  Streamwise distance between the forewing and rearwing $\frac{1}{4}-$chord positions non dimensionalised by the chord. The stagger is positive when the forewing is above the rearwing and negative when it is below the rearwing (Fig. 1.5).

- **Gap (G)**

  The absolute vertical distance that the forewing $\frac{1}{4}-$chord location is above the rearwing $\frac{1}{4}-$chord non dirnensionalised by the chord. With this definition, the gap is always positive (Fig. 1.5).

- **Decalage (δ)**

  Relative angle of attack between the upstream and downstream airfoils ($\delta = \alpha^w - \alpha^p$), where each angle of attack is taken with respect to the free stream. The decalage is therefore positive if the forewing incidence is greater than that of the rearwing or negative if the converse is true (Fig. 1.5).

1.2.2 Pros and Cons

A Flight magazine article dated April $27th$, 1944, lists the advantages and disadvantages of pure tandem aircraft, tail-first aircraft, and all-wing designs. This is a first real attempt to describe the tandem configuration, though some aspects mentioned turn out to be inaccurate, this is a good starting point for the evaluation

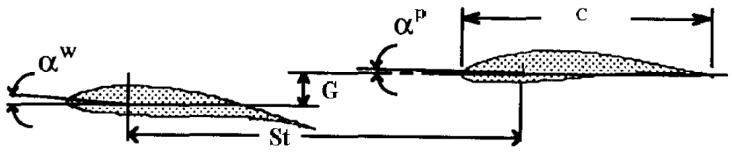

Figure 1.5: Stagger, gap and decalage [1].

of the such an unconventional configuration, which has intrigued aircraft designers since the very early days of unmanned flight.

The article lists the following.

Disadvantages

Tail-first Aircraft (canard)

1. Sensitivity to movement of the centre of gravity and to change of trim due to movement of the centre of pressure. This is likely to be quite as severe as with an orthodox aircraft.
2. Excessive side area forward of the centre of gravity. This may result in inadequate directional stability unless considerable sacrifices are made in the design to overcome the difficulty.
3. Restriction of the pilot's view by the front stabilizing surface and supporting structure. This point need only apply to comparatively small aircraft.

Tailless Aircraft (true tandem)

1. Low $C_{L_{max}}$ due in part to the difficulty of balancing the large centre of pressure shift which is associated with the more effective types of lift-increasing devices, and partly to the design compromises which are necessary to ensure a sufficient degree of stability and control.
2. Heavy control loads at low speeds on large aircraft.
3. Ultra-sensitivity to movements of the CG, resulting in very small CG range and consequent stowage problems.
4. Loss of efficiency resulting from the large wash-out which is usually needed to obtain longitudinal stability.
5. Difficulty in balancing asymmetrical application of power (engine failure on multi-engined aircraft).
6. Limited stowage space for passengers, fuel and cargo.
7. Difficulty of providing effective landing gear which will not have a tendency towards "porpoising".

8. Serious restriction of the pilot's view if the true all-wing arrangement is attempted.

Advantages

1. Both leading plane and main plane contribute to the total lift of the aircraft, and consequently the parasitic drag which is associated with the tail plane of an orthodox machine is eliminated. Tail unit drag for a clean aircraft often amounts to 10%, of the total; consequently an increase in speed of over 3%, may be obtainable.

2. With the conventional wing-tailplane system, the nose-down pitching moment which is associated with the centre of pressure movement due to increasing incidence calls for a maximum negative lift from the tail unit at the very moment when the greatest overall lift is desired. This undesirable feature is greatly aggravated when high-lift flaps are fitted; the highly efficient extending airfoil type are the worst offenders. With the layout under review the lift of the two planes is additive, and backward movement of the CP calls for an increased lift on the leading plane to maintain trim.

3. Due to the division of lift between two wings, as on a biplane, and to the possibility of achieving an increased overall C_L, a reduction in span should be possible with a consequent beneficial effect on the structure weight.

4. The elimination of the tail and the concentration of the power plant weight near the CG should also result in a considerable reduction in length and structure weight, and this feature, together with the reduction in span, should result in increased manoeuvrability.

5. The above-mentioned feature may be of great importance in connection with the gas turbine power plant where the ratio of consumable load-fixed load must be considerable higher than that associated with a reciprocating engine and airscrew. It also greatly facilitates a submerged installation in the case of a central power plant.

6. Tricycle landing gear leads itself much more readily to such a design than to the orthodox aircraft, on which poor dynamic qualities often lead to discomfort when taxiing and sometimes to structural failure. The damping effect of the front plane may make it possible to reduce the weight of the nose wheel installation.

7. The field of view is greatly improved, particularly in a single-engined arrangement where a pusher airscrew with its manifold advantages is an obvious choice. Moreover, the oil which is thrown out in such generous quantities by most constant-speed airscrews is left behind instead of obscuring the pilot's windscreen.

8. For military purposes the advantages ensuing from the use of the whole of the fuselage for stowage of the bomb load and military equipment are obvious,

while the layout is such that an almost unimpeded field of fire can be obtained. The smaller overall size, gives greater safety by reducing the target area, and the greater concentration of the load and power plants makes for economy in armour.

9. For commercial aircraft the low drag which may follow from the reduction in wetted area and parasite drag would result in greater economy of operation. The loading advantages mentioned above, aided by the absence of wing spars and supporting structure running through the fuselage at the CG of the aircraft, will make for greater convenience and comfort, while another important feature should be the maintenance of a more nearly-level floor both on the ground and throughout the flight range. It should be noted that most orthodox aircraft pass through a fairly large incidence range when taking off and landing, even if a tricycle undercarriage is fitted. The particularly good field of view for both pilot and passengers is also worth mentioning in connection with commercial applications.

1.3 Modern Day Examples

1.3.1 Home-Built

Various home-built examples of tandem wing aircraft are hereby introduced (Figure 1.6):

- **P.A.T. 1 "Pugmobile"**

  The late Howard (Pug) Piper, son of the founder of Piper Aircraft, had contracted with George Mead to develop a four-place prototype aircraft of all-composite construction, that might lead to a production aircraft.

- **Rutan Quickie**

  One of the dozens of unconventional aircraft penned by Rutan for the general aviation market, the original Quickie is Model 54 in Rutan's design series.

- **Viking Dragonfly**

  Two seater home-built aircraft designed by Bob Walters, inspired by the Rutan Quickie.

- **Q2**

  Despite their similar appearance, the $Q2$ is in a different class than the Dragonfly. Its engine is larger and its wing area is only about $2/3$ that of the Dragonfly. Thus, it was aimed more at high speed cruise.

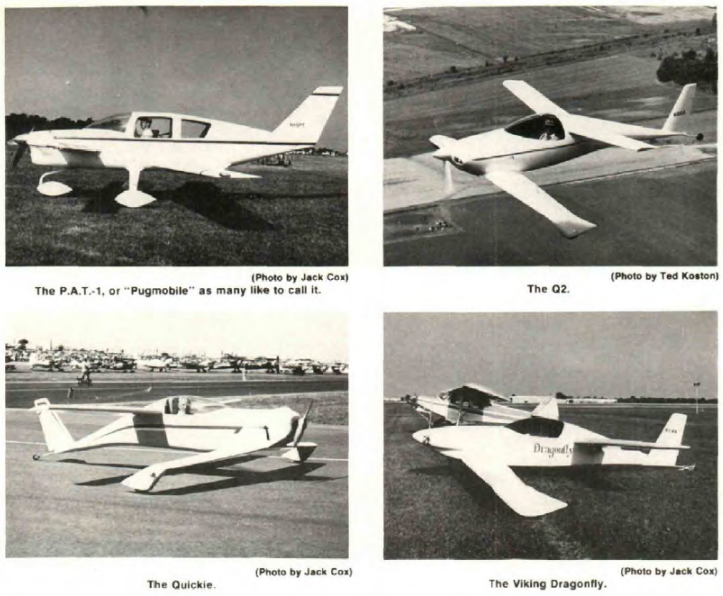

Figure 1.6: Examples of home-built tandem wing configuration aircraft [2].

1.3.1.1 BOTEC Tandem Airfoil Flairliners

Developed by Günther W. Jörg, the tandem airfoil Flairliners, apply a tandem configuration to wing in ground effect vehicles. Though the wing in ground effect never caught on, the tandem wing configuration proved to be one of the most suitable to fully take advantage of such phenomenon, as it is "...self-stabilizing and provides secure, comfortable, and high-efficiency operations...".

A primary example of Jörg's design, is the two seater $TAF\ VIII-1$ (Fig. 1.7).

1.3.1.2 Viking Dragonfly Specifications

Originally the primary objective of this work and sole inspiration for the analysis of the tandem wing configuration, the Viking Dragonfly presents specific specifications to be tested and proven efficient.

- Forewing airfoil is a variation of the $GU25-5(11)8$ (Figure 1.8).
- The rearwing airfoil is a variation of the Eppler 1212 (Figure 1.9).

1.3.2 Military

1.3.2.1 UAVs

In an attempt to achieve a highly efficient, high flying, long range, unmanned aircraft, without the need of having massive aspect ratios, which limit the operational

Figure 1.7: BOTEC Tandem Airfoil Flairliner, the two seater $TAF\ VIII-1$.

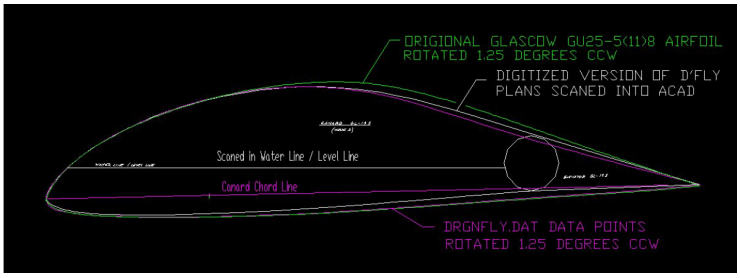

Figure 1.8: $GU25-5(11)8$ modification.

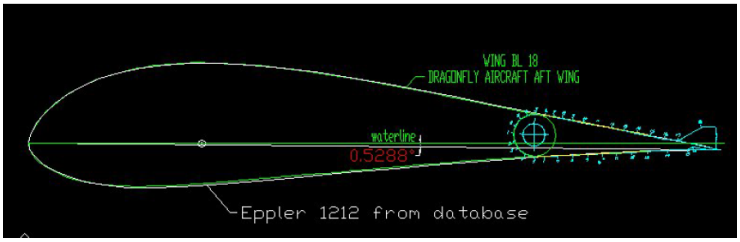

Figure 1.9: Eppler 1212 modification.

boundaries of an aircraft, as hangars are not infinitely wide, some UAV designers have turned to the tandem wing configuration. These designs include the Guizhou Soar Dragon mentioned above as a closed wing configuration example. Though not a pure tandem wing design, it does point to the fact that good UAV flight characteristics can be achieved in such configurations, with all the advantages mentioned and none of the disadvantages as they would not apply to unmanned aircraft with surveillance and intelligence missions (mostly loiter).

Other tandem wing UAV examples include:

- **Adcom Systems Yahbon and United families**

  United Arab Emirates based Adcom Systems offers a wide variety of multi mission UAVs and aerial targets. Among them pure tandem wing and VariEze inspired aircraft (Fig. 1.10).

  - United 40 and United 40 Block 5
  - Yahbon Smart Eye 1
  - Yahbon-R, Yahbon-$R2$, Yahbon-H

- **Innocon Microfalcon Lightweight UAV**

  Israeli based Innocon Ltd. offers a two model range of lightweight UAV to be launched manually through a slingshot system. The Microfalcon presents a joined wing configuration, described by Innocon themselves as a design prompted for high survivability (Fig. 1.11).

1.3.2.2 Other

Most true tandem wing configuration military aircraft were presented before or during the Second World War, these will be presented in the *History* section. The canard configuration is much more common in modern age military aircraft, including fighters, used in Russian, Chinese and European designs, and supersonic bombers.

Figure 1.10: ADCOM Systems Yahbon and United families. *Top*: United 40 Block 5 and United 40. *Middle*: Yahbon Smart Eye 1 and Yahbon-R2. *Bottom*: Yahbon-R and Yahbon-H.

Figure 1.11: Innocon Microfalcon Lighweight UAV.

Figure 1.12: North American $XB-70$ Valkyrie.

Some examples include

- Chengdu $J-10$, fighter, China (Fig. 1.13).
- Sukhoi $Su-33$, fighter, Russian.
- Dassault Rafale, fighter, France.
- Eurofighter Typhoon, fighter, Germany-Spain-UK-Italy.
- North American $XB-70$ Valkyrie, bomber, USA (Fig. 1.12).

1.3.3 Rutan Aircraft Factory and Scaled Composites

A special segment of this section must be reserved to both the Rutan Aircraft Factory and Scaled Composites, aeronautical companies founded by Burt Rutan, guru of the tandem wing and canard wing aircraft. The first specialises in home built aircraft, while the latter, prior to acquisition by Northrop Grumman, was founded to develop experimental aircraft, but now focuses on designing and developing concept craft and prototype fabrication processes for aircraft and other vehicles. It is known for unconventional designs and for its use of non-metal, composite materials.

Rutan's tandem wing creations include

Figure 1.13: Chengdu $J-10$.

- **Model** 31 **VariEze**

  A fairly high-performance homebuilt aircraft, hundreds of which have been constructed. The design later evolved into the Long-EZ and other, larger cabin canard aircraft. The Varieze is notable for popularizing the canard configuration and moldless composite construction for homebuilt aircraft (Fig. 1.14).

  Rutan's stated goals for the design included reduced susceptibility to departure/spin and efficient long range cruise; these goals were achieved. The use of a canard configuration allowed a stall resistant design, at the price of somewhat increased take-off and landing speeds and distances relative to a similar conventional design with effective flaps.

- **Model** 54 **Rutan Quickie** (Fig. 1.6, mentioned above)

- **Scaled Composites Proteus**

  Designed to investigate the use of aircraft as high altitude telecommunications relays, it set a series of world records in its category for altitude, altitude in horizontal flight, and altitude with a $1000kg$ payload.

  Due to the multi mission nature of the aircraft, it has been involved in a number of significant research projects and missions, actively marketed as a research platform, and platform for a user's guide for planning proposed missions (Fig. 1.1).

- **Rutan Voyager**

  First aircraft to fly around the world without stopping or refuelling (Fig. 1.15)

Figure 1.14: Rutan Model 31 VariEze.

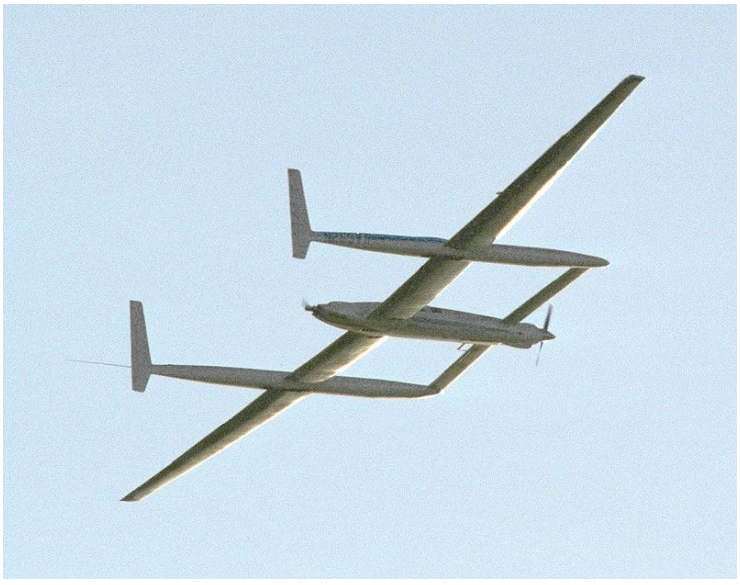

Figure 1.15: Rutan Voyager.

Part II

History

Trial and Error

Since the very early days of flight, unmanned or manned, the tandem wing configuration was believed to be a winning solution. The aircraft which were designed as tandem wing aircraft at the beginning of the $20th$ century, would show the aeronautical world just how difficult it would be to design a successful aircraft flying this type of configuration. The advent of the Second World War brought forward the resources needed for proper trials and tests on this configuration, set for aircraft with fairly different operational roles ranging from fighter-interceptor to carrier based aircraft.

Despite the advantages on paper, the tandem wing airplane struggled to obtain any operational combat role, but it did manage to capture designers' and engineers' attention in the years to come.

Chapter 2

The Langley Aerodrome

2.1 Development

2.1.1 The Smithsonian Institution

The Smithsonian Institution, established in 1846 thanks to James Smithson, the illegitimate son of the first Duke of Northumberland, died in 1829, leaving his estate to the United States of America for the establishment in Washington of an institution "...for the increase and diffusion of knowledge...". It is a group of museums and research centres administered by the United States government. Originally organized as the "United States National Museum", that name ceased to exist as an administrative entity in 1967. Termed "...the nation's attic..." for its eclectic holdings of 137 million items, the Institution's Washington, D.C. nucleus of nineteen museums, nine research centres, and a zoo—many of them historical or architectural landmarks—is the largest such complex in the world. Additional facilities are located in Arizona, Maryland, New York City, Virginia, Panama and elsewhere, and 168 other museums are Smithsonian affiliates. The Institution's thirty million annual visitors are admitted without charge; funding comes from the Institution's own endowment, private and corporate contributions, membership dues, government support, and retail, concession and licensing revenues. Institution publications include Smithsonian and Air & Space magazines.

2.1.2 Design

The Langley Aerodrome was a pioneering and successful unmanned powered flying machine, designed at the close of the $19th$ century by Smithsonian Institution Secretary Samuel Pierpont Langley, later proved unsuccessful when scaled up and fully manned. The design for both the unmanned and manned versions (Aerodrome numbers $5 - 6$ and Aerodrome A respectfully) called for a tandem wing configuration coupled with a cruciform tail (Fig. 2.1), scale and propulsion type being the only differences between the two, thus resulting in a structurally unsound airframe

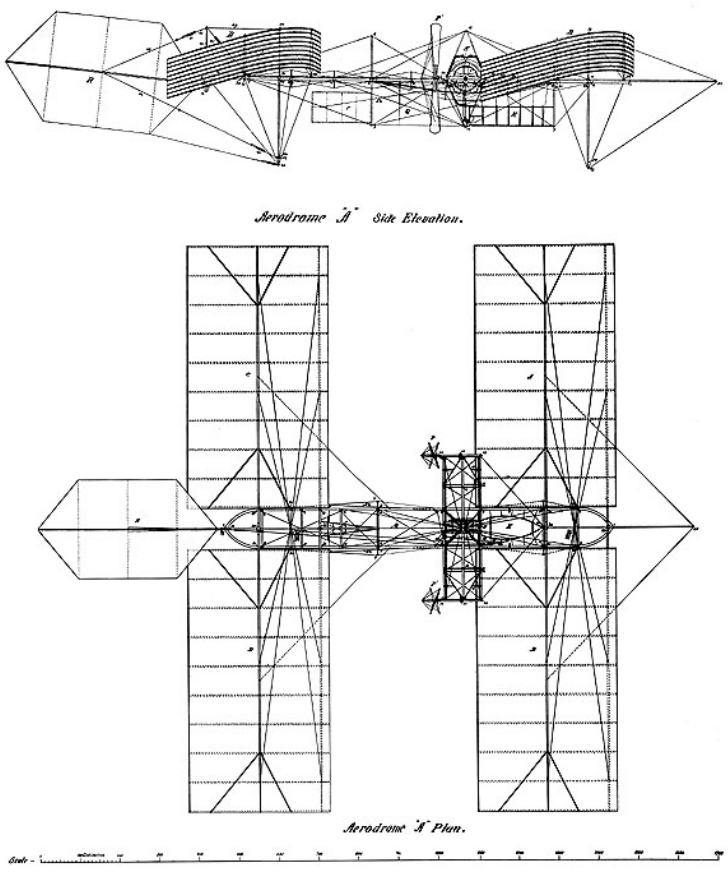

Figure 2.1: Drawings of the Langley Large Aerodrome A, 1903.

for the larger Aerodrome A. Apart from a positive wing dihedral, no attention was paid to the stability of the aircraft.

The U.S. Army paid $\$50,000$ for the project in 1898 (equivalent to about $\$1.5M$ in 2014) after Langley's successful flights with small-scale unmanned models two years earlier. Langley coined the word "Aerodrome" and applied it to a series of engine-driven unmanned and manned tandem wing aircraft that were built under his supervision by Smithsonian staff in the $1890s$ and early $1900s$. The term is derived from Greek words meaning air (aeras) running or race (dromos).

2.1.3 Flight Attempts

After a series of unsuccessful tests beginning in 1894, Langley's unmanned steam-driven model number 5 (Fig. 2.2) made a successful 90 second flight of just under a kilometre at about 40 kilometres an hour at a height of 25 to 30 meters on May $6th$, 1896.

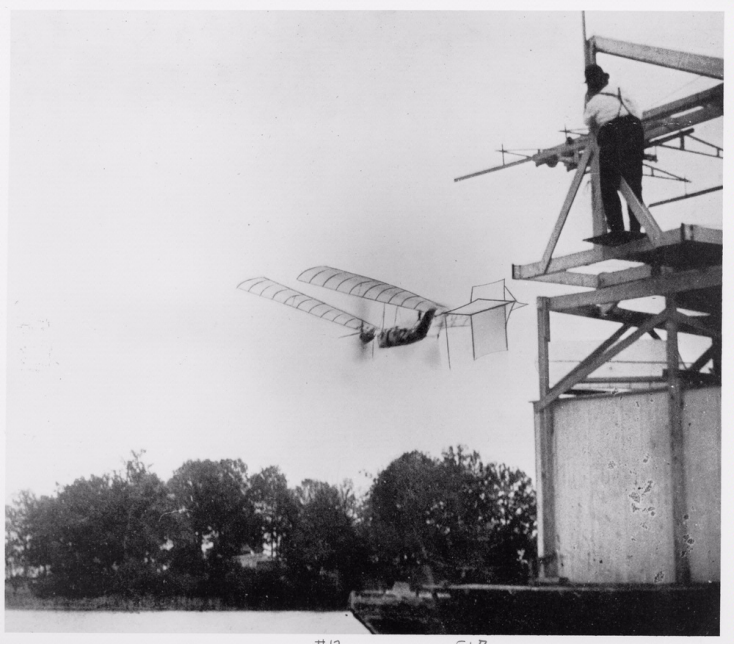

Figure 2.2: Langley Aerodrome number 5 in flight, 1896.

In November the unmanned model number 6 flew more than 1.5 kilometres. Both aircraft were launched by catapult from a houseboat in the Potomac River near Quantico, Virginia, south of Washington, D.C. The flights impressed Assistant Secretary of the Navy Theodore Roosevelt enough for him to assert that "...the machine has worked..." and to call in March 1898 for the United States Navy to create a four-officer board to study the utility of Langley's flying machine, the first documented U.S. Navy expression of interest in aviation. The full-scale manned Aerodrome (Aerodrome A), with a new and highly advanced for its time, water-cooled radial engine, financed by the United States War Department and piloted by Langley's chief assistant Charles M. Manly, was launched the same way on October $7th$ and December $8th$, 1903. On both attempts the Aerodrome failed to fly and crashed into the Potomac River seconds after launch (Fig. 2.3).

2.2 Wright Flyer's First Flight

2.2.1 Design Differences

Nine days after the December $8th$ failure (December $17th$, 1903), the Wright Brothers flew into history with their four successful flights near Kitty Hawk, North Carolina. The Flyer series of aircraft were the first to achieve controlled heavier-than-air flight, but some of the mechanical techniques the Wrights used to accomplish this

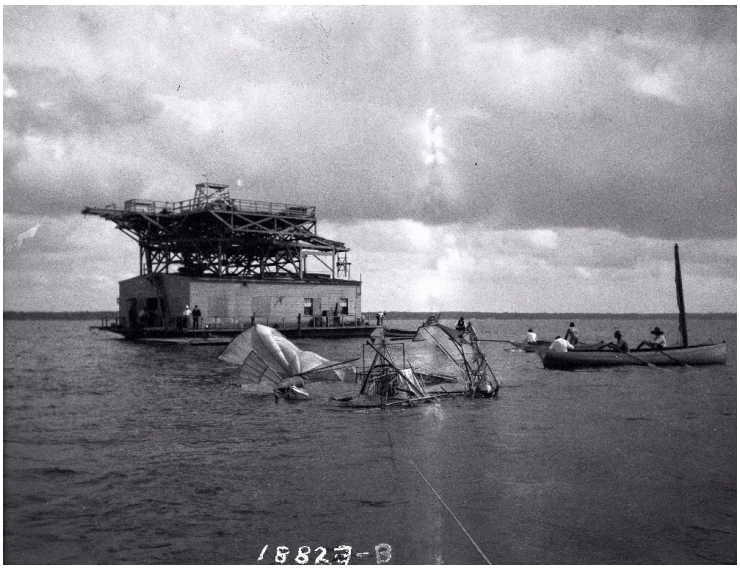

Figure 2.3: Langley Aerodrome A first flight attempt, 1903.

were not influential for the development of aviation as a whole, although their theoretical achievements were. The Flyer design depended on wing-warping and a canard for pitch control, features which would not scale and produced a hard to control aircraft. However, the Wrights' pioneering use of roll control by twisting the wings to change wingtip angle in relation to the airstream, led directly to the more practical use of ailerons by their imitators, such as Curtiss. The future of aircraft design, however, lay with rigid wings, ailerons and rear control surfaces.

The Aerodrome's internal combustion engine generated 53 horsepower, about four times that of the Wright brothers' gasoline engine of 1903. However, Langley had not properly appreciated the problems of calculating stress on an airframe or controlling an aircraft, and the Aerodrome broke up on launch. Langley made no further tests, and his experiments became the object of scorn in newspapers and the U.S. Congress. Langley's mistake was in assuming that he could simply scale up his small Aerodrome models numbers $5 - 6$ to produce a flyable airframe. Unlike the Wright Brothers, who had done extensive experiments with full-scale gliders, Langley had never tested a full-size version of his design, and was therefore unaware that the exponentially-increased drag and stresses of flight in a full-scale plane required that the airframe be very much stronger, proportionately, than any small-scale model. While his engine was more than enough to get it off the ground, Langley's airframe was far too weak to withstand the stresses of flight.

Figure 2.4: Wright Flyer's first flight, December $17th$, 1903.

Figure 2.5: Wright Flyer replica accurately presents the Wright brothers' aircraft configuration.

Figure 2.6: Curtiss modified Aerodrome, 1914.

2.2.2 Curtiss Aerodrome Modifications

With Smithsonian approval, Glenn Curtiss extensively modified the Aerodrome and made a few short flights in it in 1914 (as Samuel Pierpont Langley died in 1906), as part of an unsuccessful attempt to bypass the Wright Brothers' patent on aircraft and to vindicate Langley. Curtiss went to work, strengthening the structure, adding controls, reshaping it aerodynamically, relocating the centre of gravity, basically, making it airworthy. In 1914 he flew it for 150 feet (Fig. 2.6), and then he went back and replaced the old motor as well.

On the basis of Curtiss's reconstruction, the Smithsonian honoured Langley for having built the first successful flying machine. Based on these flights, the Smithsonian displayed the Aerodrome in its museum as the first heavier-than-air manned, powered aircraft capable of flight. This action triggered a feud with Orville Wright (Wilbur Wright had died in 1912), who accused the Smithsonian of misrepresenting flying machine history. Orville backed up his protest by refusing to donate the original 1903 Kitty Hawk Flyer to the Smithsonian, instead donating it to extensive collections of the Science Museum of London in 1928. The dispute finally ended in 1942 when the Smithsonian published details of the Curtiss modifications to the Aerodrome and recanted its claims for the aircraft (The 1914 Tests of the Langley Aerodrome. Washington, D.C.: Smithsonian Institution).

Though heavily modified by Curtiss, Langley's Aerodrome A was the first ever true tandem aircraft to achieve heavier-than-air flight.

Figure 2.7: Langley Aerodrome A at the Udvar-Hazy Centre.

2.3 Preservation

Two of Langley's scale model Aerodromes survive to this day. Aerodrome number 5, the first Langley heavier-than-air craft to fly, is on display at the Smithsonian's National Air and Space Museum in Washington, D.C. Aerodrome number 6 is located at Wesley W. Posvar Hall, University of Pittsburgh, and was restored in part by the Pitt engineering students. Fabric on the wings and tail is the only new material, although the tail and several wing ribs were rebuilt using vintage wood from the same time period provided by the Smithsonian. Langley had been an astronomy professor at the university before he ascended to the Smithsonian's top job. The man-carrying Aerodrome survived after being rebuilt and tested by Curtiss and was converted back to Langley's original 1903 configuration by Smithsonian staff. It occupied a place of honour in the Smithsonian museum until 1948 when the Institution welcomed home the original 1903 Wright Flyer from the UK. Afterwards, the Aerodrome resided out of view of the public for many years at the Paul Garber Facility in Suitland, Maryland. Today it is displayed at the National Air and Space Museum's Steven F. Udvar-Hazy Centre in Chantilly, Virginia (Fig. 2.7).

A number of individuals and groups have attempted to build reproductions of the Wright Flyer for demonstration or scientific purposes. In 1978, 23 year old Ken Kellett built a replica Flyer in Colorado and flew it at Kitty Hawk on the $75th$ and $80th$ anniversaries of the first flight there. As the $100th$ anniversary on December $17th$, 2003 approached, the U.S. Centennial of Flight Commission along with other organizations opened bids for companies to recreate the original flight. The Wright Experience, led by Ken Hyde, won the bid and painstakingly recreated reproductions of the original Flyer, plus many of the prototype gliders and kites as well as several subsequent Wright aircraft. The completed Flyer reproduction was brought to Kitty Hawk and pilot Kevin Kochersberger attempted to recreate the

Figure 2.8: A Wright Flyer replica by the American Institute of Aeronautics and Astronautics (AIAA) undergoing testing in a NASA wind tunnel.

original flight at 10:35 AM December 17, 2003 on level ground near the bottom of Kill Devil Hill. Although the aircraft had previously made several successful test flights, sour weather, rain, and weak winds prevented a successful flight on the actual anniversary date. Hyde's reproduction is displayed at the Henry Ford Museum in Dearborn, Michigan. Numerous static display-only, non flying reproductions are on display around the United States and across the world, making this perhaps the most reproduced single pioneer era aircraft in history.

Chapter 3

Early and Mid 20th Century

3.1 French Revolution

3.1.1 Blériot

Inspired by the work of Louis Blériot, who experimented with both tandem wing and monoplane configuration aircraft, many French aircraft designers of the late $19th$ early $20th$ century began experimenting themselves with such solutions. The success of the Blériot Aéronautique company met its climax in 1909 when its Type XI (Fig. 3.1) managed to be the first ever heavier-than-air aircraft to fly across the English Channel.

In 1913 Blériot acquired the assets of the Deperdussin company, following the arrest on fraud charges of its founder Armand Deperdussin. The name of the company was changed from Société de Production des Aéroplanes Deperdussin to Société Pour L'Aviation et ses Dérivés, generally referred to by its acronym, the famous SPAD comapny was born, a company responsible for the most successful and admired biplane fighters of the First World War (Fig. 3.2). Despite its monoplane success, the biplane configuration was preferred for structural reasons. The

Figure 3.1: Blériot XI, 1909.

Figure 3.2: The SPAD S.VII, 1917, flow by Italian First World War ace, Francesco Baracca (top picture), with the famous prancing horse emblem later to be adopted by Ferrari in honour of Baracca himself.

performance needed to be achieved in combat (speed, load factors and payload) required a sound structure, which monoplanes simply could not cope with at the time (all-metal construction and the cantilever wing, both having been pioneered by Hugo Junkers in 1915, became common during the post First World War period and by the $1930s$ the monoplane was fast becoming the usual configuration for a fixed-wing aircraft).

3.1.2 Pou-du-Ciel Era

The Flying Flea (Pou du Ciel literally "Louse of the Sky" in French) is a large family of light homebuilt aircraft first flown in 1933. The odd name comes from the French nickname for the Ford Model T automobile, "Pou de la Route" or "Louse of the

Figure 3.3: Pou du Ciel, 1933.

Road" because Henry Ford's economy car was so common and initially came only in black. Henri Mignet dreamed of creating a Model T of the air, an airplane for the common man, hence "Pou du Ciel" (Fig. 3.3). In the English translation, the term became "Flying Flea". Originally applied only to the $HM.14$ model, the name now describes the family of aircraft of similar configuration designed by Mignet and others, spread throughout a 60 year period (1933 to 1996).

The original Pou du Ciel had a traditional tandem wing configuration. This configuration was still not fully understood at the time in terms of flight performance, stability and control; with both wings lifting, it's hard to maintain lift balance between the two as speed changes. In a shallow dive the early versions of the aircraft would generate more lift with the aft wing and that would lift the tail, steepening the dive rapidly, beyond the ability of the front wing to lift the nose and stop the dive, at times resulting in catastrophic structural failure.

3.1.3 Further Frenchies

Further examples of French-tandem winged aircraft include the Peyret Tandem and the Peyret Taupin (Fig. 3.4), designed by Louis Peyret, a friend of Louis Blériot who helped in the design of the early Blériot models including the tandem winged Blériot VI (Fig. 3.5).

The Peyret Tandem would later be referred to as a Delanne-wing configuration. This describes a tandem wing aircraft with the rearward wing actually being an overstretched version of the horizontal tail surface. This type of design can be fully appreciated in the Arsenal-Delanne 10 aircraft, which first flew in Nazi occupied France, 1941 (Fig. 3.6). The Luftwaffe carried out a significant number of tests on the Arsenal-Delanne $10 - C2$ prototype, relocating it to Germany with the development of the Second World War.

Figure 3.4: Peyret Tandem, 1922, and a replica of the Peyret Taupin

Figure 3.5: Blériot VI, 1907.

Figure 3.6: Arsenal-Delanne 10 (top) and the 10-C2 prototype in Luftwaffe colours (bottom), 1941.

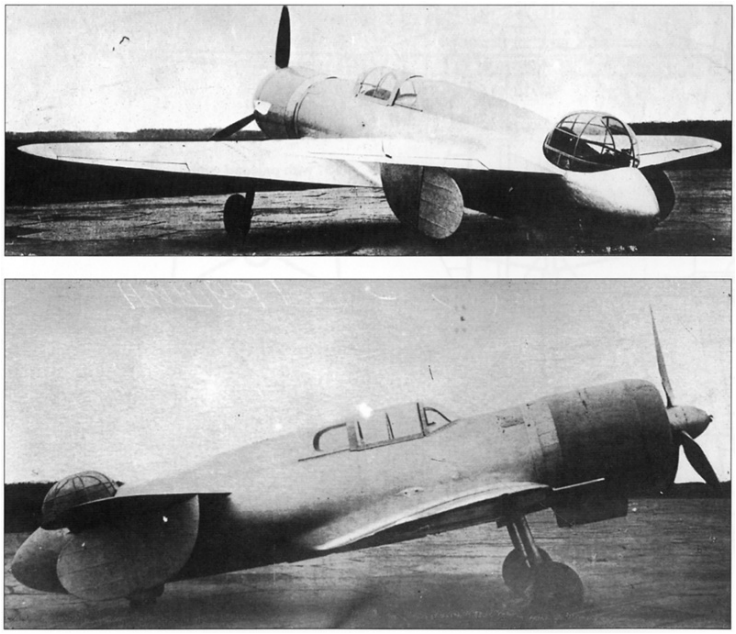

Figure 3.7: Sh-Tadem, with no vertical stabiliser on the upper surface of the rear wing, 1937.

3.2 Soviet Trials

3.2.1 Sh-Tandem

In mid-$1930s$ Soviet aviation circles were experimenting the idea of a shturmovik (storm bird in Russian), an attack aircraft capable both of strafing attacks, and limited fighter and bomber capabilities. There were two possible paths to be followed by the Soviet engineers. One was focused on what would eventually become the Ilyushin $Il-2$ and Sukhoi $Su-6$, basically a heavily armoured heavy fighter airframe fitted with guns and racks for bombs and rockets. An entirely different path was that which called for a much lighter airframe, based on single-seat fighter planes, adapted for ground attack duties. Eventually, none of the presented designs were accepted to be put in production for active service combat roles. One of these designs was Sh-Tandem designed by Pyotr Dmitrievich Grushin at the Moscow Aviation Institute (MAI).

The design was a non-conventional tandem wing aeroplane (Delanne wing). Even distribution of weight between front and rear sections allowed for more ordinance to be installed in the airframe, including a rear gunner's turret. Additionally, lack of a vertical stabiliser on the upper surface of the rear wing, allowed for wider field of fire (Fig. 3.7). At the same time the tandem wing configuration allowed for the wings to be constructed of wood rather than metal and, at least in theory,

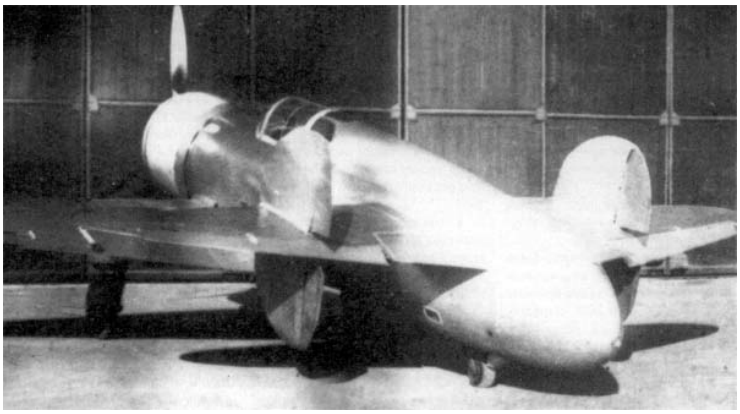

Figure 3.8: Sh-Tadem, with double vertical stabiliser on the upper and lower surface of the rear wing, 1938.

was to give the new construction unprecedented manoeuvrability. Internally the fuselage was conventional for its times: a wooden monocoque, covered in plywood with some areas covered in bakelite. Both front and rear wings were to be equipped with ailerons and elevators. This design proved to have dangerously inadequate directional (yaw) stability and had to be corrected by adding fins and rudders on the upper surface of the rear wing as well (Fig. 3.8).

There were five planned variants for the actual mounting of the stabilisers, mounted either at both ends of the rear wing, mid-span, on its lower surface or extending both on its lower and upper surfaces. Eventually the variant with vertical stabilizers on both surfaces of the rear wing was adopted as the most suitable. The serial production Sh-Tandem models were to be powered by the new Tumansky $M-88$ air-cooled radial engine. However, as they were not yet available, the prototypes used the earlier Tumansky $M-87A$ instead.

Whether a developed version could have performed better in combat than the Ilyushin $Il-2$ Shturmovik, is debatable.

3.2.2 Mikoyan-Gurevich MiG-8

The Mikoyan-Gurevich $MiG-8$ (Fig. 3.9) was a Soviet experimental aircraft. Built of wood, the aircraft was designed and built in 1945 to test canard configuration aircraft. It also used a tricycle undercarriage, the first used by the Opytnoye Konstruktorskoye Buro (Experimental Design Bureau, OKB). It was modified to test a variety of vertical stabilizer and wing tip configurations and later used as a liaison aircraft for many years by the design bureau.

Nicknamed Utka (duck), as the word canard is French for duck, the $MiG-8$ was an experimental aircraft designed and built by the OKB to evaluate the stability and handling of the canard configuration in conjunction with swept wings. This design has benefits in a jet-powered aircraft as it leaves the rear of the fuselage clear of

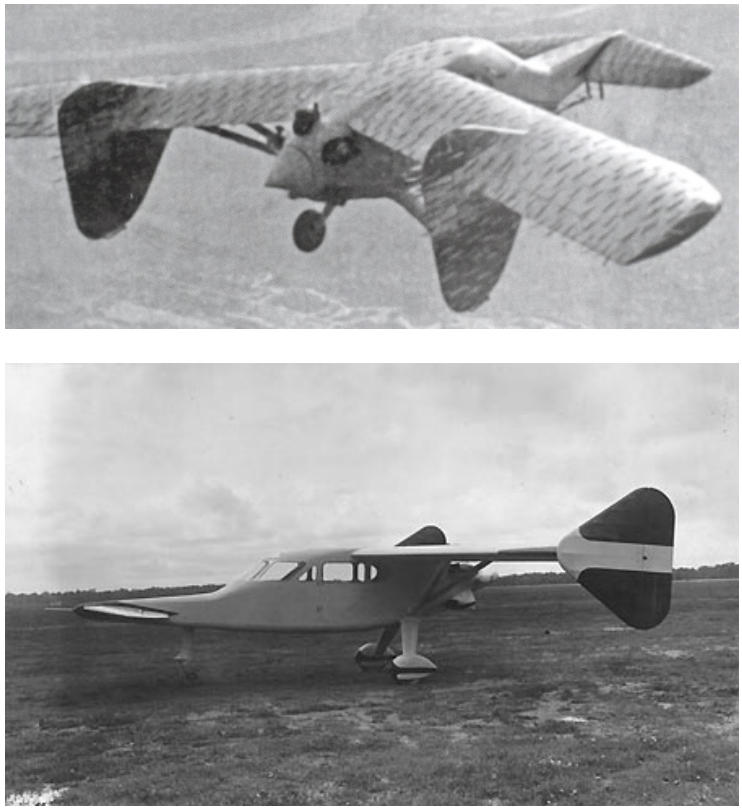

Figure 3.9: Mikoyan-Gurevich $MiG-8$, 1945.

interference from the jet's exhausts. To test the concept the $MiG-8$ was powered by a Shvetsov $M-11$ five-cylinder radial engine, with a pusher propeller. The aircraft was used as a test bed in developing the swept wing of the $MiG-15$, and afterwards continued to fly as communications/utility aircraft for the OKB. Being made of wood and fabric, it was very light and reportedly a favourite among MiG OKB test pilots for its docile, slow-speed handling characteristics.

Though not a pure tandem wing configuration aircraft, the $MiG-8$ design did prove to be mother of all Soviet/Russian built canard and swept wing configuration aircraft to follow (including the $Tu-144$).

3.3 Canard Tests - Combat Prototypes

3.3.1 SAI Ambrosini S.S.4

The SAI Ambrosini $S.S.4$ ($S.S.$ being the initials of Sergio Stefanutti, its designer) project included a canard and pusher propeller configuration. Designed as an interceptor, the $S.S.4$ never entered service due to the negative assessment of the Regia Aeronautica (Italian Royal Air Force) believed the aircraft too immature for operational use. Stefanutti was an engineer in the Regia Aeronautica at the time, who focused much of his attention on aerodynamics in order to optimize performance.

The $S.S.4$ was the last of a three-airplane series in an attempt to design a successful fighter and air superiority aircraft. Stefanutti's first experience was the $S.S.2$ model, a light aircraft with canard wings, more of a technology demonstrator, than an actual fighter. The $S.S.2$, a wooden aircraft with a small engine, essentially a powered glider, flew for the first time in 1935, and one of the two prototypes built was transformed into a two-seater model with an improved engine, and renamed the $S.S.3$ (Fig. 3.10). The experience gained in the study of aerodynamics allowed Stefanutti to devise a new version, this to be used for operational tasks: interception and air superiority. The basic configuration of the new model retained the pusher propeller, the canard, the tricycle landing gear, but was built entirely out of metal. The new model was built between 1938 and 1939 and named $S.S.4$ (Fig. 3.11) .

The $S.S.4$ was small because of its canard configuration , which needed an aerodynamically efficient shaped nose, in order to have a clean flow over the canard, and no nose-mounted motor for optimum stability and control. The aerodynamic flow was directed toward the rear, where the engine and elevons were installed. In these conditions, the flight controls would become very heavy to operate and control precision was difficult. To correct this, the engine was moved as far back as possible. The vertical stabilizers were doubled and installed on the wings, which in turn were moved towards the rear of the fuselage to allow the tail rudders to operate more effectively.

The prototype made its first flight at Eleuteri airport in Castiglione del Lago, on March $7th$, 1939. The following day, it was planned to be transferred by train to Aviano Air Base, but the chief test pilot, engineer Ambrogio Colombo, decided to make a second test flight. After a normal flight of 45 minutes, one of the elevons broke off due to a manufacturing defect, which forced the test pilot to

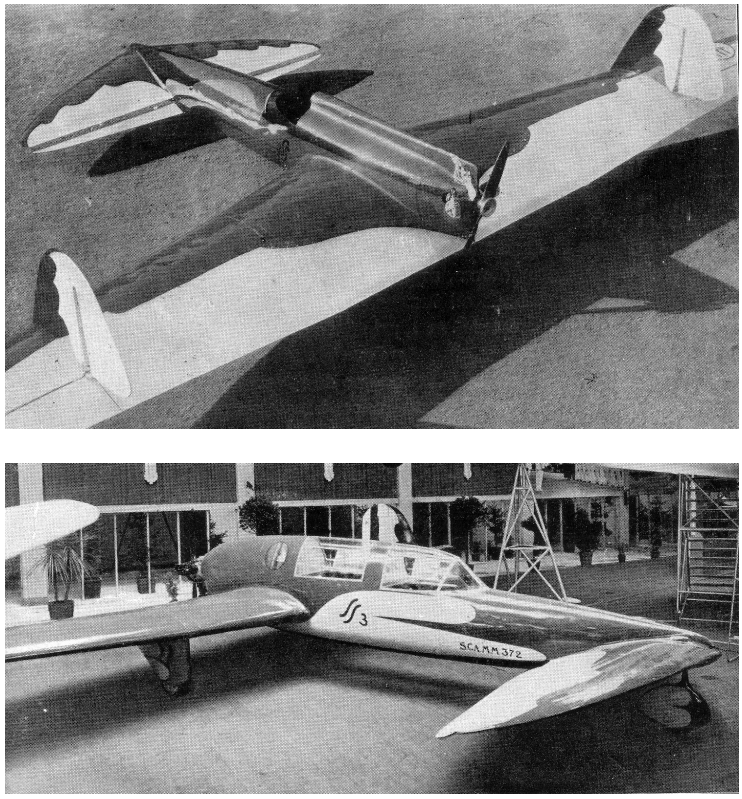

Figure 3.10: SAI Ambrosini $S.S.2$ (top) and $S.S.3$ (bottom) models, 1935.

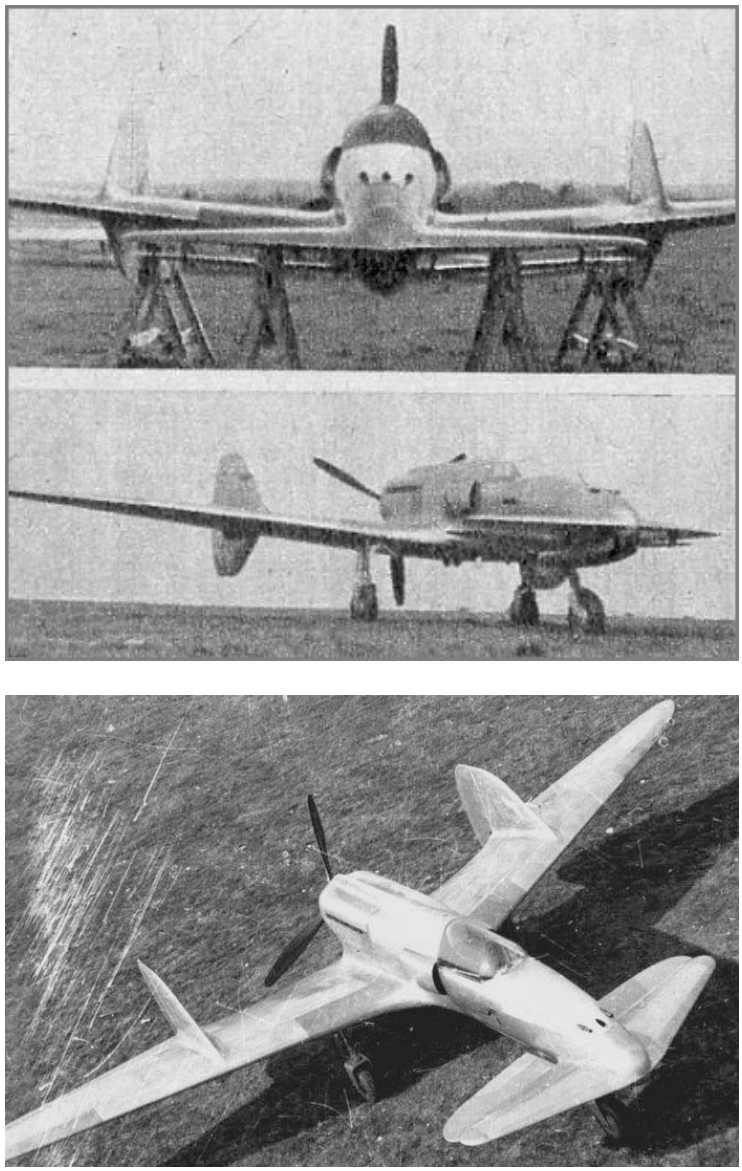

Figure 3.11: SAI Ambrosini $S.S.4$, 1939.

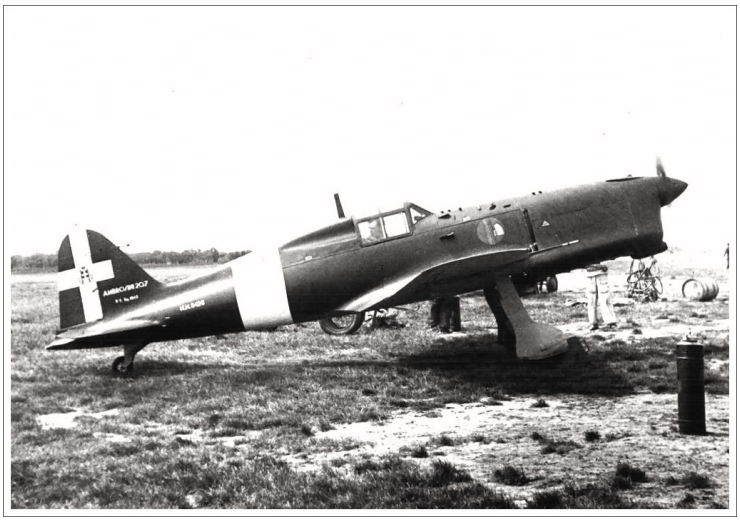

Figure 3.12: SAI Ambrosini 207, 1942.

attempt an emergency landing in a nearby field. The emergency landing turned into a fatal accident as the plane crashed directly into a tree, killing the pilot on impact. The investigation related to the accident also highlighted the excessive vibrations transmitted from the engine to the wings. This accident brought the development of the aircraft to a halt while efforts and resources were concentrated on the development of the SAI 207 (Fig. 3.12), which presented a much more traditional configuration.

3.3.2 Curtiss-Wright XP-55

The Curtiss-Wright $XP-55$ Ascender was an early $1940s$ United States prototype fighter aircraft built by Curtiss-Wright, a 1929 merge of the Curtiss Aeroplane and Motor Company and Wright Aeronautical Corporation. Ironically enough these two companies were independently started by Glenn Curtiss (who worked on modifying the Langley Aerodrome A making it airworthy) and by the Wright Brothers, respectfully. Along with the Vultee $XP-54$ and Northrop $XP-56$, it resulted from United States Army Air Corps proposal issued on November $27th$, 1939 for aircraft with improved performance, armament and pilot visibility over existing fighters; it specifically allowed for unconventional aircraft designs. The $XP-55$ (Fig. 3.13) featured, much like its predecessor, the $S.S.4$, a canard configuration, a rear mounted engine, swept wings and two vertical tails. Because of its pusher propeller design, it was sarcastically referred to as the "Ass-ender". It would also be the first Curtiss fighter aircraft to use tricycle landing gear.

On June $22nd$, 1940, the Curtiss-Wright company received an Army contract for preliminary engineering data and a powered wind tunnel model. The US Army Air Corps (USAAC) was not completely satisfied with the results of these tests,

Figure 3.13: Curtiss-Wright $XP-55$ Ascender, 1943.

and Curtiss-Wright took it upon itself to build a flying full-scale model which it designated $CW-24B$. It had a fabric-covered, welded steel tube fuselage with a wooden wing. The undercarriage was non-retractable. On July $10th$, 1942, the United States Army Air Forces issued a contract for three prototypes under the designation $XP-55$. During the mock-up phase, it was decided to switch to a more powerful $1,275hp$ engine. A special feature of the $XP-55$ was a propeller jettison lever located inside the cockpit to prevent the pilot from hitting the propeller during bailout.

The first $XP-55$ was completed on July $13th$, 1943 and had the same aerodynamic configuration as the final prototype. The aircraft made its first test flight on July $19th$, 1943 from the Army's Scott Field near the Curtiss-Wright plant in St Louis, Missouri. Initial testing revealed that the take off run was excessively long. To solve this problem, the canard elevator surface area was increased and the aileron up trim was interconnected with the flaps so that it operated when the flaps were lowered. On November $15th$, 1943, test pilot Harvey Gray testing the stall characteristics on the first prototype at altitude, suffered a sudden flip over on the aircraft's back and plummeted in an uncontrolled, inverted descent. The pilot was unable correct the aircraft's attitude as it achieved a $4,900m$ loss of altitude before Gray was able to safely bail out. The aircraft crashed and was destroyed (Fig. 3.14).

The second $XP-55$ was similar to the first but with an even larger canard elevator, modified elevator tab systems, and a change from balance tabs to spring tabs on the ailerons. It flew for the first time on January $9th$, 1944. All flight tests were restricted so that the stall zone was avoided. The third $XP-55$ flew for the first time on April $25th$, 1944. It was found that the aircraft's stall characteristics could be greatly improved by the addition of wingtip extensions, and by increasing the limits of the canard elevator excursion. Between September $16th$, and October $2nd$, 1944, the second $XP-55$, which had been modified to the same standards as the third aircraft, underwent official USAAF flight trials. The performance of the $XP-55$ was not very impressive and was often inferior to that of more conventional

Figure 3.14: First $XP-55$ crashed during stall characteristics test flight, 1943.

fighter aircraft already in service. In addition, by 1944 jet-powered fighter aircraft were already well on their way in their development and were soon scheduled to become operational. Hence all development of the $XP-55$ was scrapped.

3.3.3 Kyushu J7W

Another canard configuration prototype example was the Kyūshū $J7W1$ Shinden (Magnificent Lightning), a Second World War Japanese propeller-driven aircraft. In contrast with the rest of the canard configuration Second World War prototypes, the Shinden was scheduled to be put into production, but never achieved an active combat role as it was developed in the last months of the war. The configuration, again similar to that of the $S.S.4$, called for wings attached to the tail section and canard stabilizers, and a pusher propeller configuration. Developed by the Imperial Japanese Navy (IJN) as a short-range, land-based interceptor, the $J7W$ was a response to $B-29$ Superfortress raids on the Japanese home islands. The Shinden (Fig. 3.15) was expected to be a highly manoeuvrable interceptor, but only two prototypes were finished before the end of war. The building of a gas turbine–powered version was considered, but never even reached the drawing board.

The idea of a canard-based design was brought forward by Lieutenant Commander Masayoshi Tsuruno, of the technical staff of the IJN in early 1943. Tsuruno believed the design could easily be retrofitted with a turbojet engine, when a suitable variant could become available. His ideas studied and developed by the First Naval Air Technical Arsenal (Dai-Ichi Kaigun Koku Gijitsusho), which decided to follow Stefanutti's plan to first test a glider version of the aircraft. Hence three

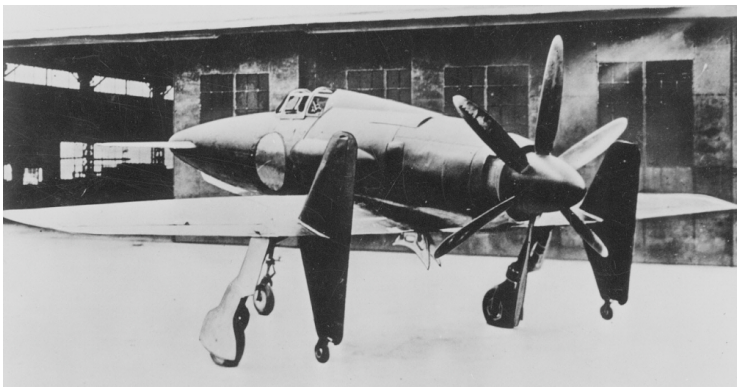

Figure 3.15: Kyūshū $J7W1$ Shinden, 1945.

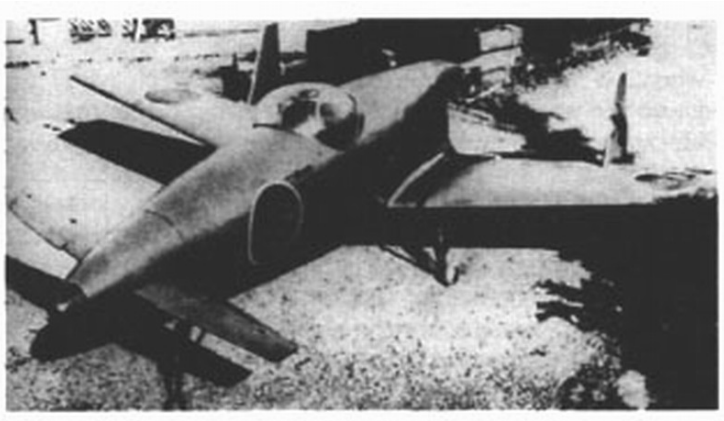

Figure 3.16: Yokosuka $MXY6$, 1943.

gliders were designed and designated Yokosuka $MXY6$ (Fig. 3.16).

One of the gliders was later fitted with a $22hp$ 4-cylinder air-cooled engine (similar to the $S.S.2$, which was fitted with an $18hp$ engine). The feasibility of the canard configurations was proven by both the powered and unpowered versions of the $MXY6$ by the end of 1943, and the Navy was so impressed by the flight tests, that they instructed the Kyushu Aircraft Company to design a canard interceptor based on Tsuruno's concept. The first prototype was completed in April 1945. Even before the first prototype took to the air, the Navy had already ordered the $J7W1$ into production, with quotas of 30 Shinden a month given to Kyushu's Zasshonokuma factory and 120 from Nakajima's Handa plant. It was estimated some $1,086$ Shinden could be produced between April 1946 and March 1947.On August $3rd$, 1945, the prototype first took off, with Tsuruno at the controls, from Itazuke Air Base. Flights were successful, but showed a marked torque pull to starboard (due to the powerful engine), some flutter on the propeller blades, and

vibration in the extended drive shaft.

Japan's formal surrender took place on September $2nd$, 1945, less than a month after Shinden's first flight.

3.3.4 Mizuno Shinryu

The Mizuno Shinryū/Jinryū (Divine Dragon), was yet another Japanese designed late Second World War canard configuration aircraft. Where the Shinden was considered to become primarily a combat interceptor, the Shinryu was designed as a rocket-powered Shimpu mission aircraft or interceptor. With Japan's situation worsening, the project never proceeded beyond the initial phase of development, possibly due to more prominent projects; $J8M$ or $Ki-200$, Kikka, and $Ki-201$.

Again the need for a new concept of aircraft was induced by the constant $B-29$ Superfortress incursions over Japanese mainland. The concept was exactly the same as that of the Kyushu $J7W$ Shinden. A point defence interceptor that could quickly rise to meet the bombers, and so the Mizuno Shinryū was born (Fig. 3.17).

However, the development of the Shinryū began with designs for a far more conventional aircraft. In November 1944, the Kaigun Koku Hombu looked into the possibilities of an aircraft to undertake shimpu missions (Shimpu is an alternative reading with more solemn characters, forming the word Kamikaze). The aircraft being studied would be a glider in a conventional configuration launched with rocket boosters from caves or shore positions and pilots would guide the aircraft and its $100kg$ explosive payload into Allied ships or tanks should the Japanese home islands be invaded. A number of concepts were discussed and sketched and after much deliberation the design was completed by May 1945, and Mizuno, a small aircraft manufacturer, had almost finished the prototype. This design proved to be unsuitable for such missions, so the canard configuration Shinryu was developed instead (as a pure interceptor).

The Shinryū would never be built because the end of the war terminated any further work on the design. Likewise, the Jinryū glider would never fly under power. After the failure of the rocket motors during ground tests, the war came to a close before more suitable and reliable motors could be acquired and tested. Mizuno completed a total of five Jinryū gliders.

3.4 Tandem Tests - Combat Prototypes

3.4.1 Westland P.12 Lysander Delanne

The Westland Lysander was a sturdy aircraft with STOL abilities, generally used for army co-operation work and liaison purposes, usually unarmed aircraft primarily used by military forces for artillery observation or transporting commanders and messages (Fig. 3.18), produced by Westland Aircraft (later to become Westland Helicopters). By late 1940 it was obsolescent, but production was extended until 1942 in the belief that new uses could be found for such aircraft.

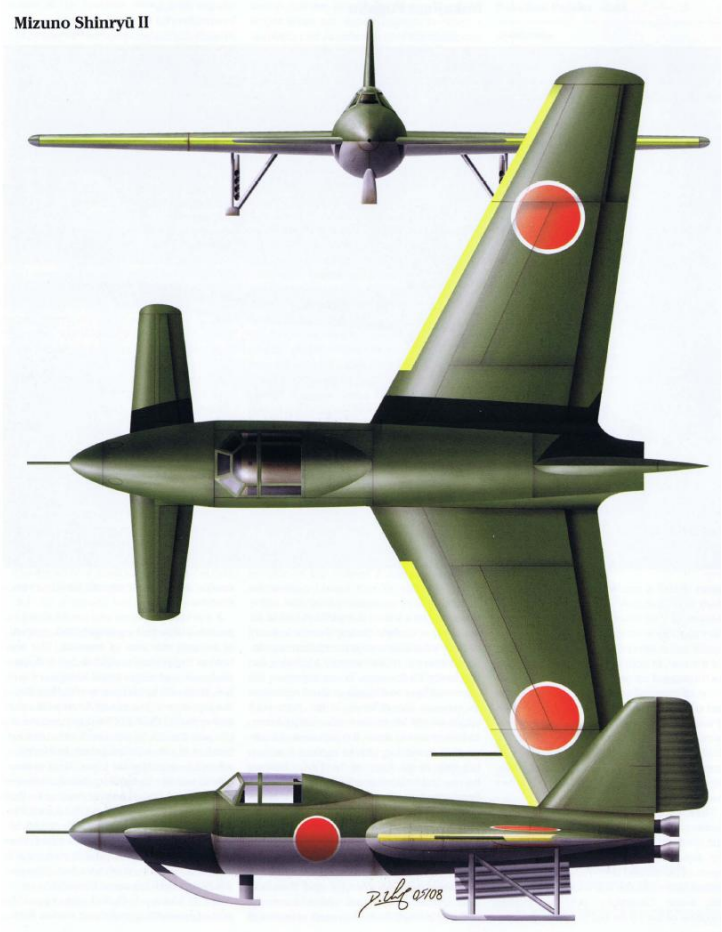

Figure 3.17: Mizuno Shinryu artist's impression.

Figure 3.18: RAAF Westland Lysanders in formation during an observation mission over the Suez canal, 1940.

The Lysander proved to be especially suitable for clandestine delivery of Allied agents into occupied France, and RAF 419 Flight, (later recommissioned as 1419 Flight) made good use of the Lysander until late 1941, when, after becoming 138 Squadron (Special Duties, formed to undertake missions for the Special Operations Executive to maintain clandestine contact with the French Resistance), it had only two operating aircraft deployed to Tangmere in great secrecy.

A further and more relevant variant of the Lysander was the $P.12$ Delanne model (Fig. 3.19), which featured a Delanne wing needed for the housing of a tail turret as to adapt the aircraft to its new role of turret night-fighter. This meant fitting a second wing in tandem (Delanne wing) to the main one with end-plate fins and rudders. The aircraft became a kind of hybrid, an army-co-operation aircraft with a heavy bomber tail unit.

The aircraft underwent trials in the winter of $1940 - 41$. Radical changes to the rear fuselage enabled a mock-up of a four-gun Nash & Thompson turret to be installed, made of plywood and perspex and having a very light framework. It was hoped the design would develop into an effective night-fighter, or at least a gunnery trainer. However, the Lysander turret night-fighter, despite successful flight trials, remained a one-off experiment.

3.4.2 Miles' Libellula

3.4.2.1 M.35

While contemplating the problems related to carrier borne combat aircraft, as they require wing-folding systems, which increase the aircraft's weight at the expense of payload and the adaptations of single-engined tail-dragger land-based aircraft, which typically had poor visibility when landing, George Miles in 1941 visited the Aeroplane and Armament Experimental Establishment at RAF Boscombe Down,

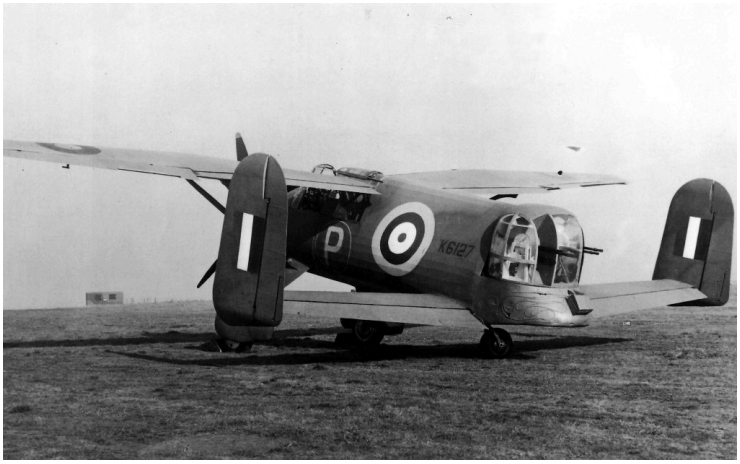

Figure 3.19: Westland $P.12$ Lysander Delanne $K6127$ turret night-fighter, 1941.

where he saw the Westland $P.12$ Lysander Delanne. Miles realised that a tandem-wing fighter could be built to fit onto carrier elevators without folding and that the pilot could be seated in the nose section, giving an excellent view for carrier landings. Among the solutions considered, the tandem wing configuration appeared to Miles to be the answer, provided it was aerodynamically feasible.

The result was a small wooden aircraft with a high-set front wing and low-set rear wing, fixed tricycle undercarriage, and pusher propeller, with the engine in the rear of the fuselage and the pilot sitting in the front of the fuselage, the Miles $M.35$ (Fig 3.20). Much like its predecessors, the $M.35$ suffered from stability issues as the flight characteristics of tandem wing aircraft had still not been fully understood. These problems were to be later investigated through the use of extensive wind tunnel tests on the $M.35$ itself. The test results were then adopted to design a new species of Miles' tandem aircraft, the $M.39$.

3.4.2.2 M.39

The larger $M.39$ was drawn up as a twin-engined design prepared to meet certain specifications issued by the Air Ministry for a high speed bomber. The M.39 would have a crew of three in a pressurized cabin, a bomb-bay amidships, and carry two fixed $20mm$ cannon in the roots of the forward wings. To prove the concept Miles designed and built a $\frac{5}{8}th$ scale version, the $M.39B$ (Fig. 3.21), which flew on July $22nd$, 1943, showing none of the undesirable handling characteristics encountered with the $M.35$.

Much interest was shown by the authorities in part due to the unorthodox design for such a large aircraft. The rear wing was higher than the forward wing to avoid downwash undesired effects and give ground clearance for the propellers. The Ministry of Aircraft Production agreed a development contract and purchase of the M.39B. Miles continued testing, generating more flight data and submitted an im-

Figure 3.20: Miles $M35$, 1942.

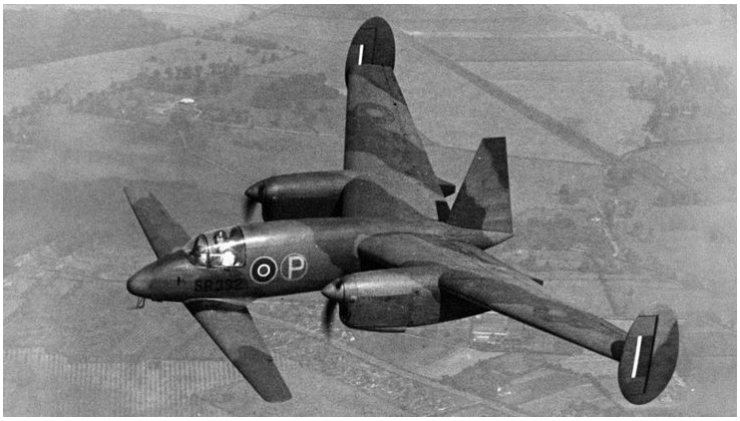

Figure 3.21: Miles $M.39B$ concept, 1943.

proved $M.39$ design in early 1944. Meanwhile the sole $M.39B$, serial number $SR392$, was delivered to the Royal Aircraft Establishment at Farnborough in 1944, were it suffered two flight accidents and later scrapped with the cancellation of the full-sized bomber project.

Part III

Literature Review

Research

A much more detailed and precise approach was needed to properly develop, enhance, and exploit the advantages derived from tandem wing configurations, as these are only obtained through specific investigation and thorough testing. Such studies include wind tunnel testing and computational fluid dynamics both applied to $2D$ and $3D$ set ups, varying from oscillating airfoils to Delanne wings.

The research criteria and study parameters also vary widely. From geometric characteristics (varying both locally and in spanwise direction) such as the horizontal stagger, vertical gap, and the decalage angle, to specific mission objectives such as high efficiency (coupled to the lowering of induced drag), greater manoeuvrability and/or enhancing aircraft performance. These parameters, in relation to the home-built market, do also take into account the possibility of designing a low cost, low complexity but highly exciting, radical, non conventional aircraft.

The articles presented were extracted from a vast choice of papers concerning tandem wings and/or airfoils. The ones presented are thought to be the most relevant in the field of tandem wing aircraft conceptual design. The first articles presented refer to a three dimensional and two dimensional computational study of the geometric optimisation of the tandem wing configuration, to then move on to experimental work (non computational), and finally to the study of varying performance of this non conventional design.

Chapter 4

Geometric Optimization: Gap, Stagger, Decalage

4.1 3D CFD

4.1.1 Dual and Single Wing Design Integration

The most interesting work done in such matter is presented by Rokhsaz and Selberg [23] as a collection of previous works and studies done on a pair of $MS(1)-0313$ transonic airfoils and with the use of both $2D$ and $3D$ numerical simulation confirm the findings of the cited articles. Through the use of vortex panel and vortex lattice codes, the authors are able to accurately mimic results achieved by their predecessors.

- Airfoil: $MS(1)-0313$ (transonic airfoil)
- $2D$ Method: Multi element vortex panel program (thesis work).
- $3D$ Method: Vortex lattice method, C_{l_0} and C_{l_α} from vortex panel program.
- Optimization: Nastran-Semobeam.
  - $2D$ Kaplan method.
  - $3D$ Prandtl-Glauert-Goethest.

4.1.1.1 Method

This article is a collection of data and results presented in other papers, illustrating the advantages of the dual wing design configuration versus that of the single wing. This is a brief report presenting the most relevant results presented in the article. Even if the results obtained are not directly comparable to the thesis case study, the methodology applied and the results presentation is to be thoroughly followed if not copied altogether.

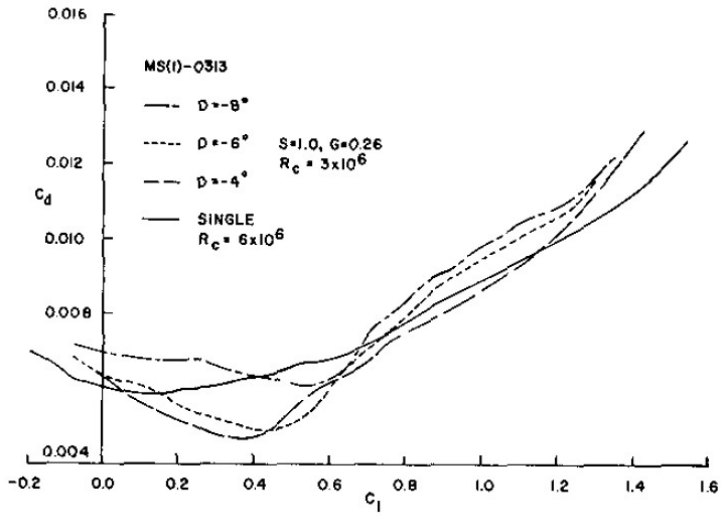

Figure 4.1: C_d versus C_l for single and dual wing at varying decalage [23].

- Airfoil: $MS(1) - 0313$ (transonic airfoil)
- $2D$ Method: Multi element vortex panel program.
- $3D$ Method: Vortex lattice method, C_{l_0} and C_{l_α} from vortex panel program.
- Optimization: Nastran-Semobeam.
  - $2D$ Kaplan method.
  - $3D$ Prandtl-Glauert-Goethest.

4.1.1.2 Results

Aerodynamic efficiencies of two classes of dual wing aircraft were studied and compared with the performance of optimum equivalent single wing designs. In all cases, using numerical techniques, the dual wing configurations were optimized for the best combinations of decalge, critical Mach number, and Reynolds number. In every respect, the dual wing systems proved to be more efficient . These studies were limited to constant engine and fuel weights. - Lower power requirements of the dual wing configurations can allow lowering these weights. These reductions can further improve the performance of these systems. Additionally, new airfoil shapes optimized for dual wing operation could further improve the dual wing configuration advantage over the single wing configuration.

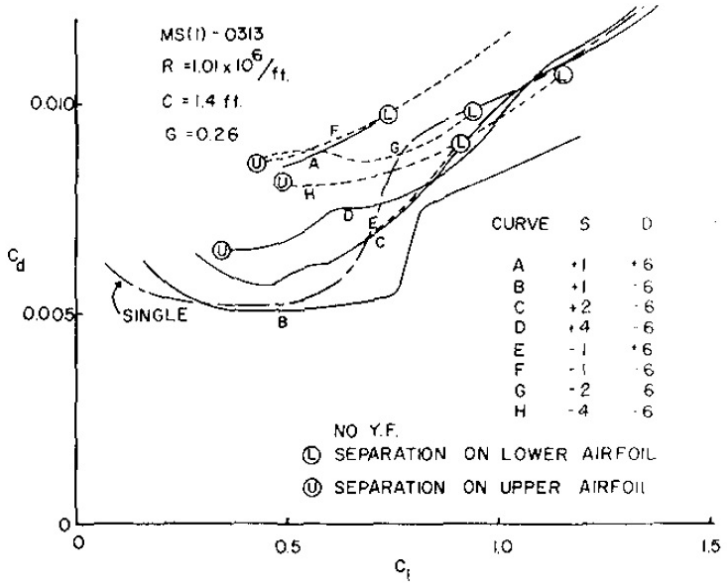

Figure 4.2: Stagger versus decalage [23].

4.1.2 A Study of Lift for a Tandem-Biplane Wing Configuration

Another noticeable example is the work of Molina, Garcia, Fuentes, and Herrera [24] on a simulated Henry Mignet's "Pou du Ciel" (Figure 4.5) configuration. Their work consists in the use of an application of the lifting surface method of vortex-rings on the assumption of incompressible potential flux (code which was verified against wind tunnel experimental data). Resulting in the fact that all considered geometric factors, but that of wing inflexion, may have a significant effect on C_L and $C_{L_{alpha}}$ values.

4.1.2.1 Method

Based on a previous code developed in Garcia's work "Analysis of tandem-biplane wing code by the lifting surface method of vortex-rings", the method yields a set of equations on the basis of the classic Laplace's equation and of suitable boundary conditions, modified for the "Pou du Ciel" configuration (Fig. 4.6).

The method is then summarised in:

$$\begin{matrix} a_{ij} & b_{in} \\ c_{mj} & d_{mn} \end{matrix} \begin{matrix} \Gamma_j \\ \Gamma_n \end{matrix} = \begin{matrix} RHS_i \\ RHS_m \end{matrix} \tag{4.1}$$

where the set of influence coefficients of each wing on itself are a_{ij} and d_{mn}, those of each wing on the other are b_{in} and c_{mj}, and the vectors Γ are the two sets of

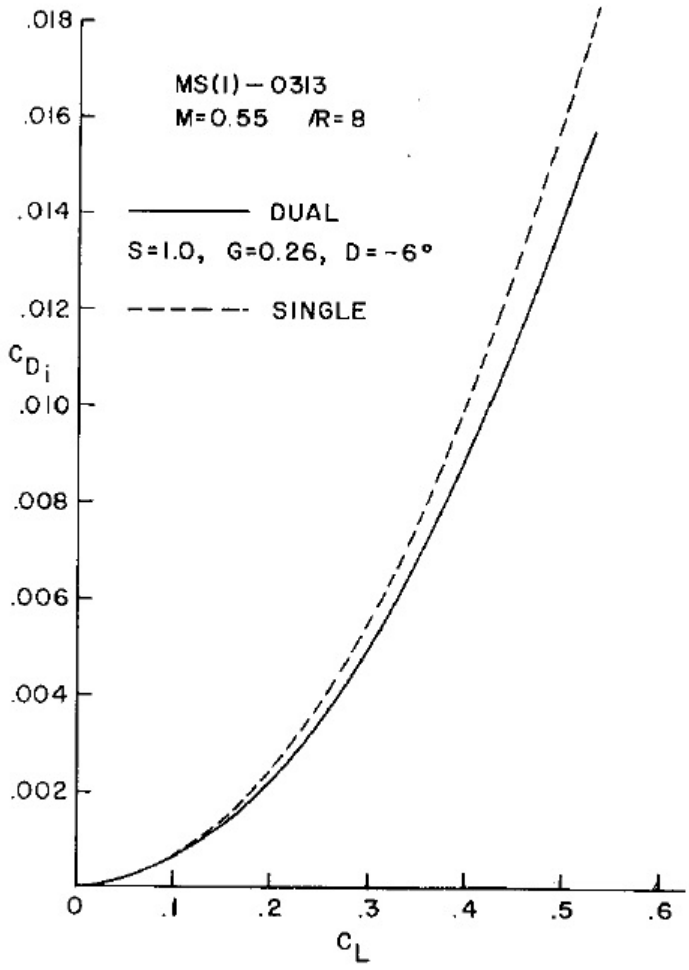

Figure 4.3: Induced drag for single versus dual wing [23].

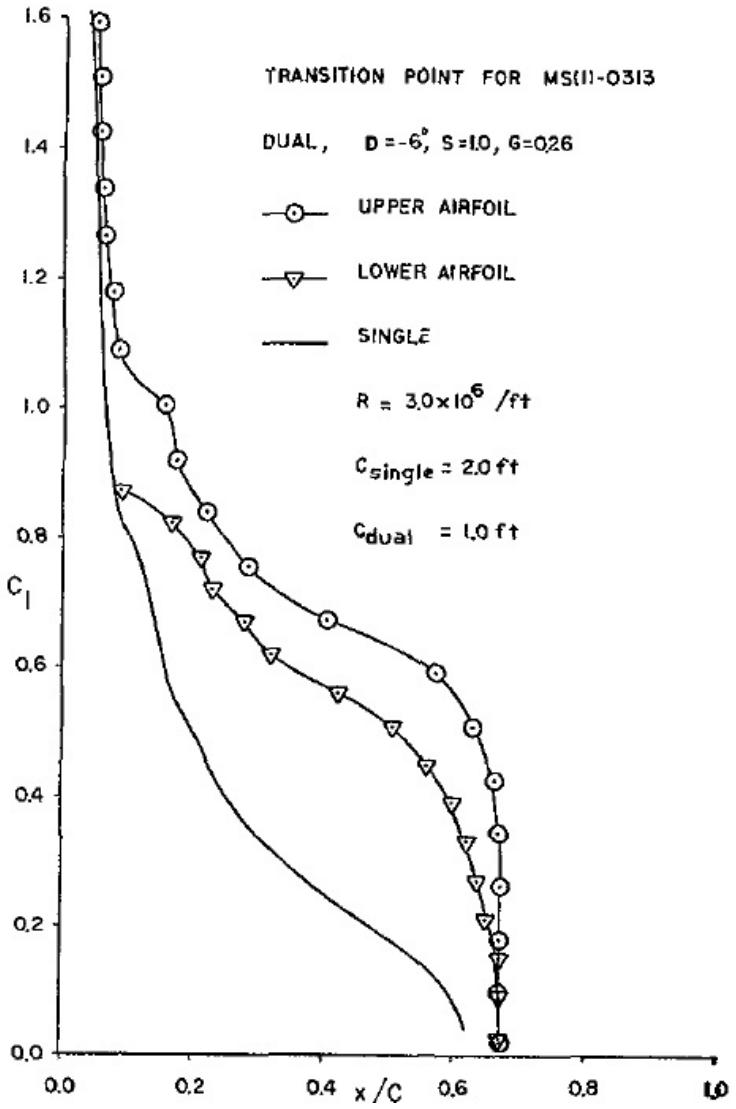

Figure 4.4: Transition point for single versus dual wing [23].

Figure 4.5: Henry Mignet's "Pou du Ciel" (Flying Flea) [24].

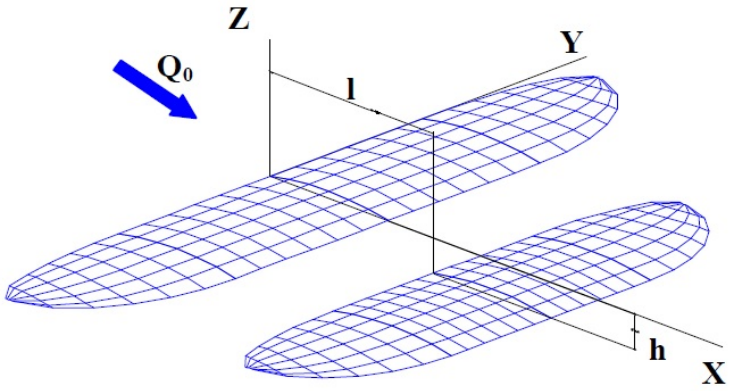

Figure 4.6: Schematics of the studied model in "Pou du Ciel" configuration [24].

unknowns vortex-ring flows, each for one wing. RHS are sets of constant values that depend on the external free-flow condition before interaction with wings

The developed code was verified against wind-tunnel experimental data from Rebuffet's work [37], from 1966, which studied a $2D$ set up. For this purpose the layout adopted was that described in Fig. 4.7. The results of this verification are shown in Fig. 4.8, and shows that the developed code was validated for a range of angle of attack between -4° to about 12°. Once the code had been verified, seven test variables were selected and tested out within a specific range of values (Fig. 4.9, along with a control scenario), which included, gap (h/c), stagger (l/c), decalage ($\delta_1 - \delta_2$), fore and aft wing span (b_1 and b_2) and inflexion (fraction of semi-span for which wing geometry goes from straight to semi-elliptical measured from YZ plane). A second test consists of maintaining constant gap and stagger, while varying the other factors as well as testing different value combinations (Fig.

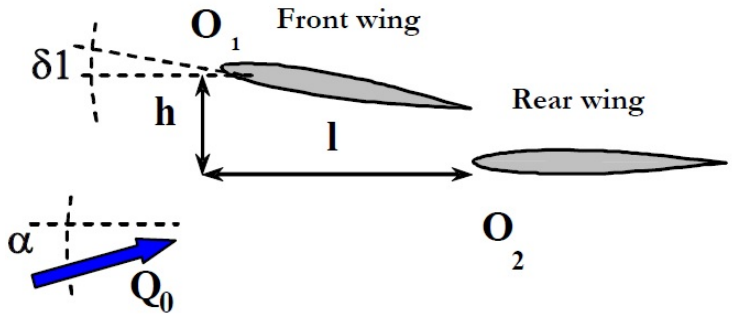

Figure 4.7: Plane cell for computer code verification [24].

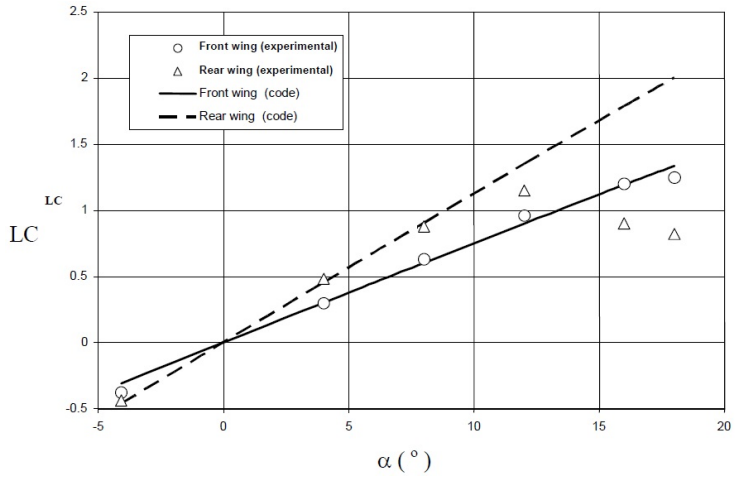

Figure 4.8: Lift coefficient in each wing versus angle of attack [24].

4.10).

4.1.2.2 Results

The first trials, with all factors selected varying, suggested that four factors were of importance to the studied response (δ_1, b_1, b_2, and inflexion), while the other three were not. However, the follow up experiment, with constant gap and stagger, indicated that one of the seemingly important factors from the first experiment would have no effect (inflexion). Hence a contradiction arises from this study, which comes from inference done on limited knowledge, and on the false assumption of no interaction-effect in the design (Fig. 4.11).

The authors' conclusions are that the results suggest that all "geometric" factors (except inflexion) may be of importance for LC values and C_{l_α} coefficient. Factors δ_1, b_1, b_2 and their interactions may have substantial effects on the lift.

Run	h/C	l/C	δ1	δ2	b1	b2	inflexion
1	1	1	1	1	1	1	1
2	1	1	1	2	2	2	2
3	1	2	2	1	1	2	2
4	1	2	2	2	2	1	1
5	2	1	2	1	2	1	2
6	2	1	2	2	1	2	1
7	2	2	1	1	2	2	1
8	2	2	1	2	1	1	2

Level	h/C	l/C	δ1	δ2	b1 [m]	b2 [m]	Infl.
1	0	-1	-3°	-3°	6	4	0.5
2	1	1	+3°	+3°	10	6	0.7

Figure 4.9: Test matrix with value assignments for each test (top) and high and low value definitions for each variable (bottom) [24].

Level	inflexion	δ1	b1/b2
1	0,5	-3°	1
2	0,7	3°	2,5
Constant parameters	**h/C**	**l/C**	**δ2**
	1	1	0°

Run	Column
inflexion	1
δ1	2
inflexion x δ1	3
b1/b2	4
inflexion x b1/b2	5
δ1 x b1/b2	6
inflexion x δ1 x b1/b2	7

Figure 4.10: Test matrix with value assignments, at constant gap and stagger (top) and high and low value definitions for each variable and the combinations assigned (bottom) [24].

Run	CL1	CL2	Clα [1/rad]
1	2,872	7,632	*4,794*
2	2,995	8,668	*5,138*
3	7,847	2,121	*4,984*
4	6,873	1,902	*5,428*
5	5,037	5,629	*5,211*
6	4,204	6,146	*5,175*
7	5,849	4,647	*5,396*
8	5,755	4,994	*4,447*

Run	LC1	LC2	Clα [1/rad]
1	5,861	4,738	*5,299*
2	5,771	5,025	*5,554*
3	6,237	4,836	*5,537*
4	6,140	5,331	*5,905*
5	5,856	4,729	*5,292*
6	5,772	5,015	*5,550*
7	6,231	4,827	*5,529*
8	6,140	5,320	*5,900*

Figure 4.11: Test results. All variable factors (top) and constant gap and stagger (bottom) [24].

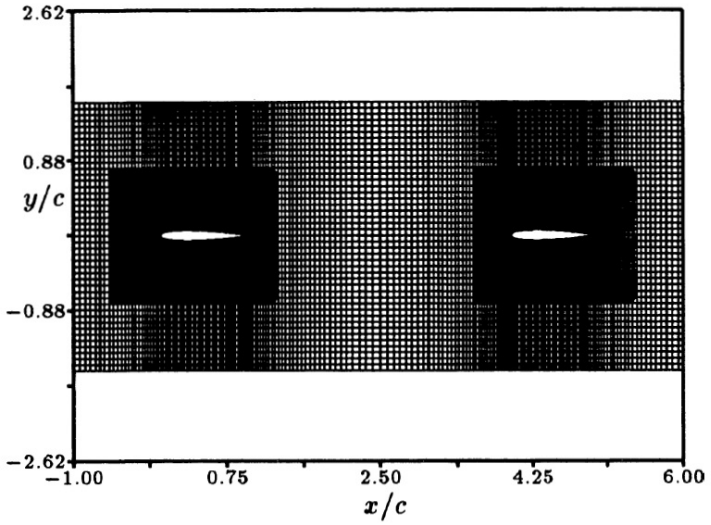

Figure 4.12: Analysis layout. Computational grid for tandem airfoil geometry [25].

4.2 2D CFD

4.2.1 Numerical Simulations of Tandem-Airfoil Aerodynamics

In Fanjoy and Dorney's work [25], time dependent Navier Stokes equations are applied on a pair of $NACA\ 0012$ airfoils (at both low and high speed). Their horizontal stagger and decalage angle vary while in search of an optimum solution to substantially increase overall aerodynamic efficiency. The vertical gap is kept constant at zero and effects of increasing stagger and varying angles of attack are evaluated.

4.2.1.1 Method

Fanjoy and Dorney apply a two-dimensional Navier-Stokes analysis, which had been previously applied for turbo machinery applications. This analysis was then modified to predict external flow fields related to airfoil geometry. This work was then compared and verified with experimental data presented by Abbott and Von Doenoff in [34], and Holst in [35]. Tandem configuration at varying stagger and decalage angles results, were compared with the results from the isolated airfoil, in order to quantify any increase in aerodynamic performance (Fig. 4.12).

The validation phase consisted of testing the isolated $NACA\ 0012$ airfoil both at low speed and high speed. The results can be seen in Fig. 4.13, and these show excellent agreement in the values for lift and a fair agreement in the values for drag.

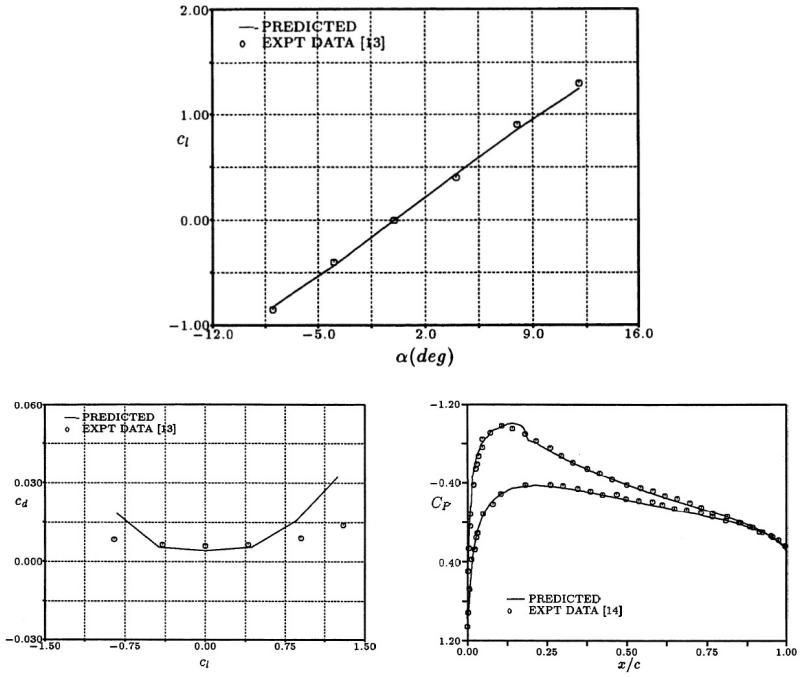

Figure 4.13: Data validation for the isolated $NACA\ 0012$. Lift coefficient versus angle of attack (top), drag coefficient versus lift coefficient (bottom left), and surface pressure coefficient distributions (bottom right) [25].

FORE α(deg)	AFT α(deg)	FORE c_l	AFT c_l	FORE c_d	AFT c_d
-8.00	-7.61	-0.9780	-0.7697	0.0092	0.0294
-4.00	-3.80	-0.4960	-0.3697	0.0032	0.0084
0.00	0.00	-0.0010	-0.0001	0.0013	0.0014
4.00	3.81	0.4943	0.3686	0.0031	0.0083
8.00	7.63	0.9770	0.7693	0.0091	0.0288

FORE α(deg)	AFT α(deg)	FORE c_l	AFT c_l	FORE c_d	AFT c_d
-8.00	-6.49	-0.8834	-0.8029	0.0147	0.0301
-4.00	-3.23	-0.4475	-0.3891	0.0049	0.0094
-2.00	-1.59	-0.2236	-0.1652	0.0025	0.0031
0.00	0.00	-0.0005	-0.0004	0.0017	0.0014
2.00	1.59	0.2237	0.1647	0.0025	0.0031
4.00	3.23	0.4473	0.3896	0.0048	0.0077
8.00	6.49	0.8892	0.8077	0.0141	0.0239

FORE α(deg)	AFT α(deg)	FORE c_l	AFT c_l	FORE c_d	AFT c_d
-8.00	-6.79	-0.8377	-0.8956	0.0168	0.0173
-4.00	-3.58	-0.4410	-0.4337	0.0052	0.0057
-2.00	-1.78	-0.2216	-0.1843	0.0027	0.0028
0.00	0.00	-0.0004	-0.0004	0.0019	0.0019
2.00	1.78	0.2213	0.1855	0.0026	0.0029
4.00	3.59	0.4439	0.4220	0.0050	0.0063
8.00	7.19	0.8772	0.8586	0.0148	0.0185

Figure 4.14: Lift and drag coefficients for $NACA\ 0012$ in tandem configuration for varying angles of attack and stagger. $St/c = 2.0$ (top), $St/c = 3.0$ (middle), and $St/c = 4.0$ (bottom) [25].

4.2.1.2 Results

Results show that there is an optimum stagger distance associated with maximum airfoil performance. For moderate to large stagger distances, the rear airfoil performs similar to the forward airfoil at low angles of attack, which was predictable thanks to downwash effects (Fig. 4.14).

4.2.2 The Effect of Wing Spacing on Tandem Wing Aerodynamics

A similar study is presented by Broering and Yongsheng Lian [26]. They too rely on Navier Stokes equations for the numerical analysis of flapping tandem airfoil configurations. Their tests concentrate on low Reynolds Number ($Re = 5000$) for the purpose of studying tandem wing configurations to be applied on MAV (micro air vehicles) aircraft. Stagger varies, while other parameters are kept constant.

4.2.2.1 Method

The flow problems were solved using the time dependent incompressible Navier-Stokes equations on flat plates in tandem configuration, a form of which is:

$$u_t + (u \cdot \nabla)\, u + \frac{\nabla p}{\rho} = \nu \Delta u \tag{4.2}$$

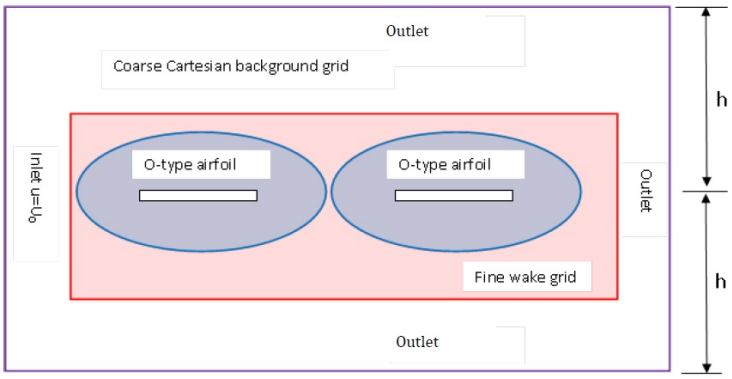

Figure 4.15: Layout and scheme of the computational grid used for tandem wing analysis [26].

$$\nabla \cdot u = 0 \tag{4.3}$$

where u is the flow velocity, p is the pressure, ν is the kinematic viscosity and ∇ represents the Poisson operator. The flow was assumed to be accurately modelled as a direct numerical simulation and no turbulence model was employed. For the flapping problem, a dynamically updated overlapping grid was adopted, as developed by Henshaw and Schwendeman in [36].

The study carries out an investigation over the effect of wing spacing (stagger) for the tandem configuration of the flat plates and compares it to the single plate scenario over time. The wing spacing varies between a maximum of $1.0c$ and $0.1c$, with a plate thickness of $0.05c$.

4.2.2.2 Results

The results obtained, confirm the theoretical advantages of a tandem wing configurations. The authors describe that, compared to twice the value of a single wing, the tandem configuration produced noticeably more thrust, significantly less lift and only a slightly smaller resultant across all staggers tested.

Ignoring the conclusions coming from the flapping movement of the airfoils, which exceed the purpose of this paper, test results concur with the work done by Fanjoy and Donrney, where an optimum stagger distance is deemed to exist.

4.3 3D Experimental

4.3.1 Experimental Determination of Improved Aerodynamic Characteristics Utilizing Biplane Wing Configurations

Olson and Selberg [27] carried out investigations to determine if the aerodynamic characteristics of biplane wing systems could be made more efficient for low subsonic

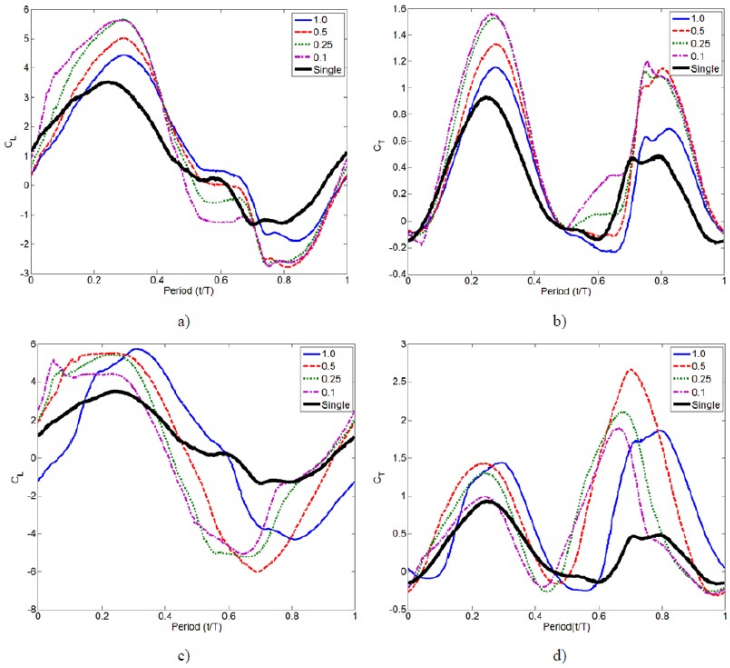

Figure 4.16: Lift coefficient for the tandem configuration at different wing spacings compared to a single wing. *a)* Forward wing lift, *(b)* forward wing thrust, *(c)* rear wing lift, and *(d)* rear wing thrust [26].

speeds than those of a monoplane of comparable area and similar aspect ratio. A variable position three-dimensional biplane wing system and a fuselage that could be fitted with a monoplane wing or the variable position biplane wing system were tested in the University of Missouri-Rolla subsonic wind tunnel.

4.3.1.1 Method

To study the effect of improving the aerodynamic characteristics of an airplane through a detailed study of a biplane wing configurations and its characteristic parameters. As described by Olson and Selberg, specifically, the study aims to:

1. Investigates the aerodynamic characteristics of a three-dimensional biplane cell, using non symmetrical airfoils, by varying the gap, stagger, and decalage angle.
2. Establishes maximum lift coefficient, maximum lift over drag, and drag coefficient at a cruise angle of attack, as a function of gap, stagger, and decalage angle.
3. Determines wing efficiencies, and effects of the biplane on range and endurance over the monoplane.

For this purpose, test models were constructed out of steel, brass, aluminium, cast epoxy, basswood, balsa wood, and fibre tubing. The airfoil selected for all aircraft configurations is a $NACA\ 2412$ (Fig. 4.17) and since this study is concerned with aerodynamic characteristics of biplane configurations, the models were fabricated to have the same lift capacity and hence wing areas, and as similar induced drag characteristics as possible.

Tests carried out at the University of Missouri-Rolla subsonic wind tunnel, consisted in a set of biplane wings at various combinations of gap, stagger, and decalage angle. The fuselage was tested, first, with a monoplane wing and eventually, with the biplane wings. All tests were conducted, due the nature of the model support system, starting at an angle of attack of 20ř and working toward -6ř in 2ř decrements. For each angle of attack, normal, axial, pitching force, and temperature measurements of the atmosphere surrounding the test area were recorded concurrently.

4.3.1.2 Results

Advantages of varied biplane configuration over the single wing configuration are summarized in Figure 4.19, where St in the horizontal stagger, Ga is the vertical gap, and De is the decalage angle.

Which brings to the following conclusions, with respect to the change from monoplane to biplane-tandem configuration:

- Maximum of 25% drag reduction.
- Significant efficiency rise.
- Pitching moment characteristics significantly improved.

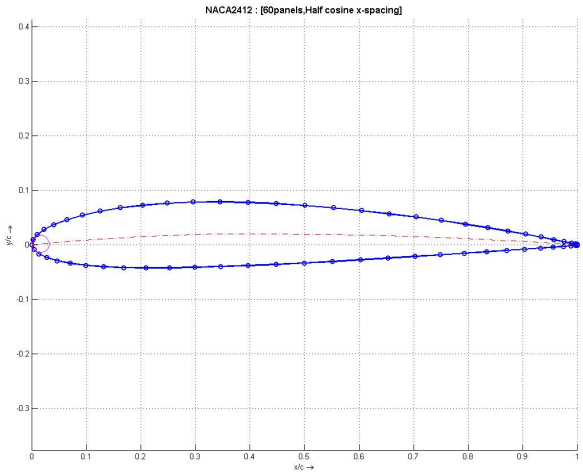

Figure 4.17: $NACA\ 2412$ airfoil.

4.4 2D Experimental

4.4.1 An Experimental Study of a Closely Coupled Tandem Wing Configuration at Low Reynolds Numbers

Testing for low Re closely coupled tandem airfoil configuration was brought forth by Scharpr and Mueller [1] inherent to RPV (remotely piloted vehicles) development. Using the Wortmann $FX63-137$ airfoil (Fig. 4.20) as a study case, with flow visualization techniques using kerosene smoke.

4.4.1.1 Method

All of the aerodynamic experiments were performed in the South subsonic wind tunnel at the University of Notre Dame Aerospace Laboratory. Flow visualization using kerosene smoke was performed to compliment the quantitative data. This provided some insight to the physics of the flow and facilitated analysis of the force and pressure data. Both airfoils were mounted vertically in the test section (Fig. 4.21), allowing aerodynamic force measurement of a single airfoil. This airfoil was varied in angle of attack while the second airfoil was held at a constant incidence.

The airfoil attached to the balance was rotated in angle of attack from -15ř to 20ř and back to 0ř in order to record any aerodynamic hysteresis effects.

4.4.1.2 Results

Results obtained are presented in Figure 4.22, where s represents the single airfoil, w the aft airfoil and c the fore airfoil (canard). The results do show that some

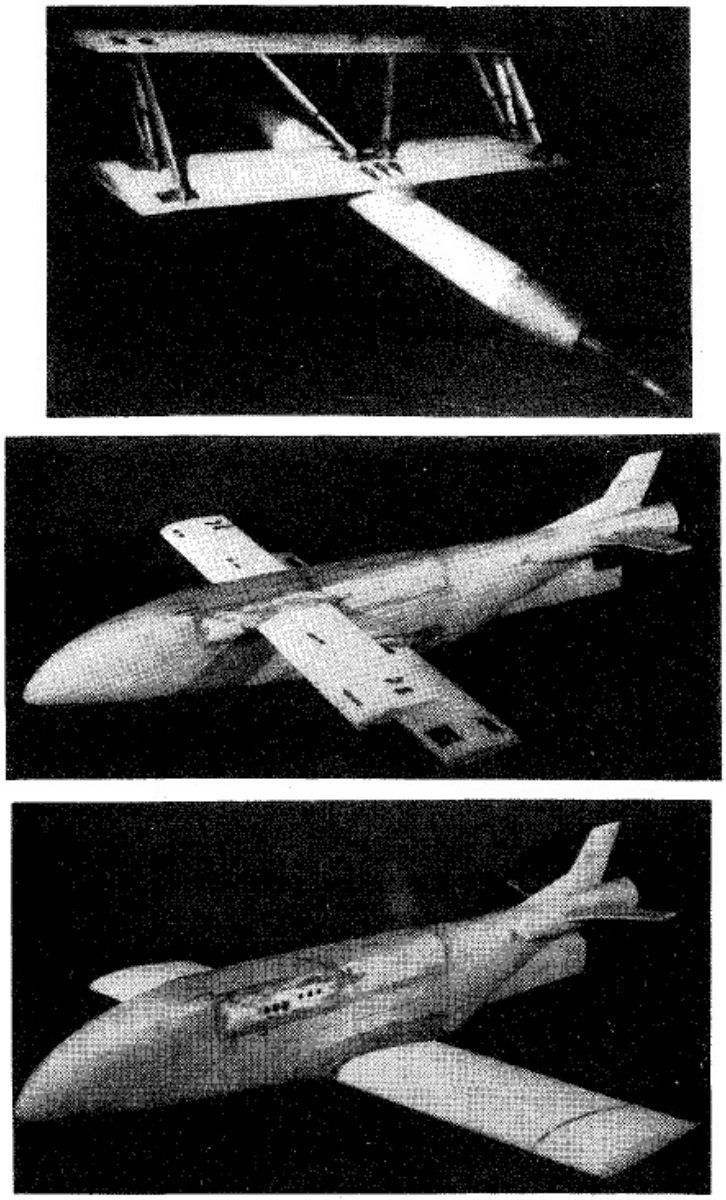

Figure 4.18: Three test models used, biplane, fuselage-biplane, and fuselage-monoplane [27].

Configuration	L/D_{max}	$\Delta(L/D_{max})$ (%)	C_D ($C_L = 0.175$)	ΔC_D (%)	$C_{L max}$	$\Delta C_{L max}$ (%)
Monoplane	8.988	0	0.028	0	0.943	0
Biplane Case I GA = 1.0 ST = 0.875 De = −6 deg	10.49	+16.7	0.021	−25	0.722	−23.4
Biplane Case II Ga = 1.0 St = 0.875 De = −5 deg	11.788	+31.2	0.022	−21.4	0.734	−22.2
Biplane Case III Ga = 0.875 St = 1.0 De = −6 deg	10.449	+16.3	0.024	−14.3	0.840	−10.6

Figure 4.19: Summary of aerodynamic characteristics for three biplane wing systems and their comparison with monoplane [27].

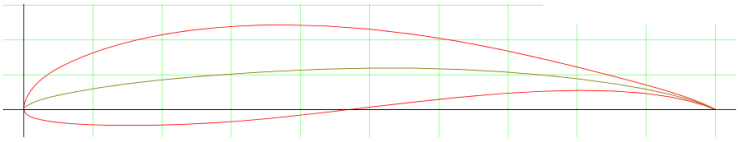

Figure 4.20: Wortmann $FX63-137$ airfoil.

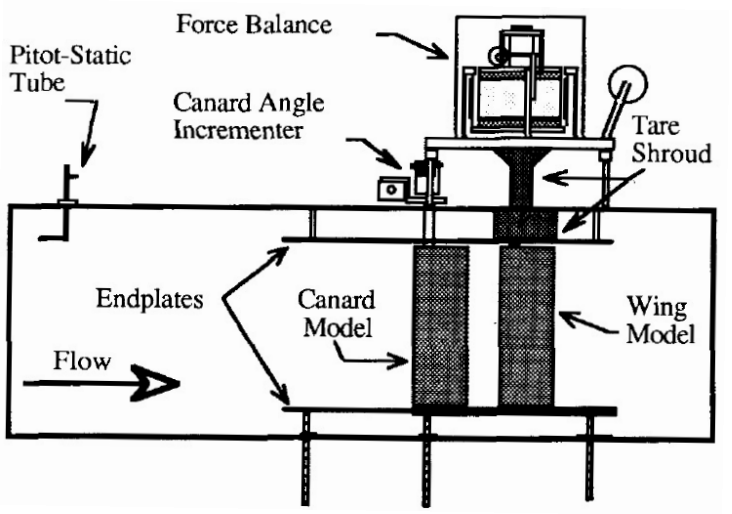

Figure 4.21: Force balance testing arrangement [1].

α			C_l				C_d				L/D			
s	w	c	s	w	c	tot	s	w	c	tot	s	w	c	tot
0°	0°	0°	0.359	0.251	0.449	0.700	0.032	0.030	0.040	0.070	11.088	8.477	11.153	10.000
0°	0°	5°	0.359	0.320	0.879	1.199	0.032	0.026	0.063	0.089	11.088	12.502	13.929	13.472
0°	0°	10°	0.359	0.133	1.382	1.515	0.032	0.020	0.088	0.108	11.088	6.827	15.729	14.028
5°	5°	0°	0.686	0.545	0.532	1.077	0.065	0.056	0.039	0.095	10.507	9.723	13.694	11.337
5°	5°	5°	0.686	0.694	1.035	1.729	0.065	0.052	0.054	0.106	10.507	13.340	19.124	16.311
5°	5°	10°	0.686	0.427	1.548	1.975	0.065	0.034	0.072	0.106	10.507	12.382	21.482	18.632
10°	10°	0°	1.383	0.822	0.680	1.502	0.082	0.102	0.028	0.130	16.776	8.054	23.973	11.554
10°	10°	5°	1.383	1.040	1.166	2.206	0.082	0.098	0.039	0.137	16.776	10.594	30.111	16.102
10°	10°	10°	1.383	0.639	1.584	2.223	0.082	0.081	0.043	0.123	16.776	7.890	37.159	18.073

Figure 4.22: Force Coefficients For Tandem Wing and Single Airfoil Measurements [1].

advantages over a single wing design can be gained by utilizing a closely coupled tandem wing arrangement (in this $2D$ arrangement).

The authors, supported by their data, come to the conclusion that since increased performance is unique to the requirements of the application, the benefits or disadvantages of using any of these configurations will correspond solely to each specific design requirement. Therefore, one cannot simply say that one configuration is better than an other, except when a specific performance requirement is identified.

Chapter 5

Performance

5.1 3D CFD

5.1.1 Design of a New Tandem Wings Hybrid Airship

Through the numerical method, a new tandem wing hybrid airship with both higher utility value and economy efficiency was obtained in a study by Li Feng, Ye Zheng Yin and Gao Chao [28]. Their work concentrates on improving lift-drag characteristics. A code was implemented for the optimization design for aerodynamic configuration of tandem wings hybrid airship via the response surface method. RANS (Reynolds Averaged Navier Stokes) models are used for such numerical simulation.

5.1.1.1 Method

This tandem wing configuration is a hybrid airship as describe in Fig. 5.2. Lift comes from both wing generated lift, through $NACA\ 0030$ airfoil (Fig. 5.1), and buoyancy, with the use of lighter than air gas (helium) in the airfoil's cavity. Numerical simulation carried out by three-dimensional compressible Reynolds-Averaged Navier-Stokes equations and regardless of the impact of the gravity of air and mass diffusion, the simplified control differential equations, whereas static lift (buoyancy) is calculated by Archimedes Law.

5.1.1.2 Results

The results indicate that the tandem wings hybrid airship has considerable volume efficiency and higher aerodynamic characteristics. After optimization, the lift-drag ratio of this hybrid airship was increased by 6.08%. In a given gross lift condition, tandem wings hybrid airship may provide more payload and specific productivity. Furthermore, the size of tandem airship is smaller so the demand for skin flexible materials can be reduced.

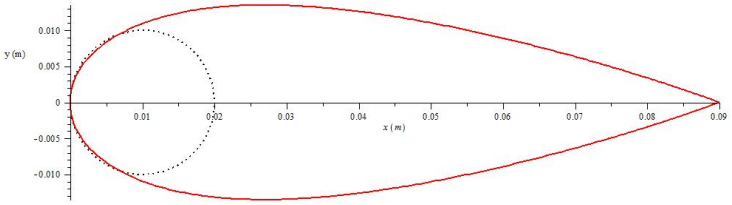

Figure 5.1: $NACA\ 0030$ airfoil.

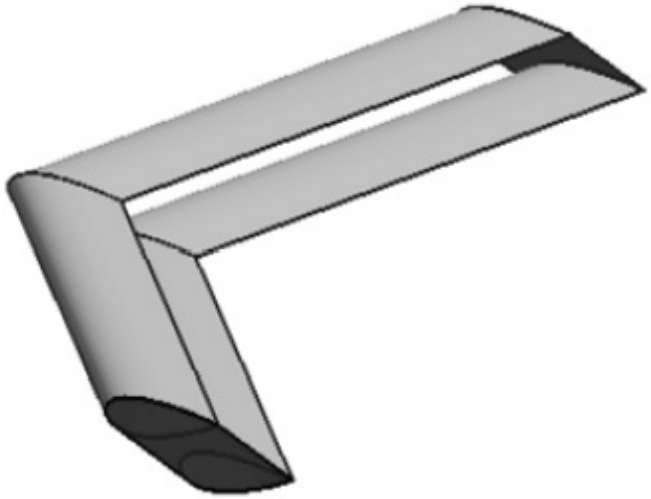

Figure 5.2: Tandem wing configuration hybrid airship layout [28].

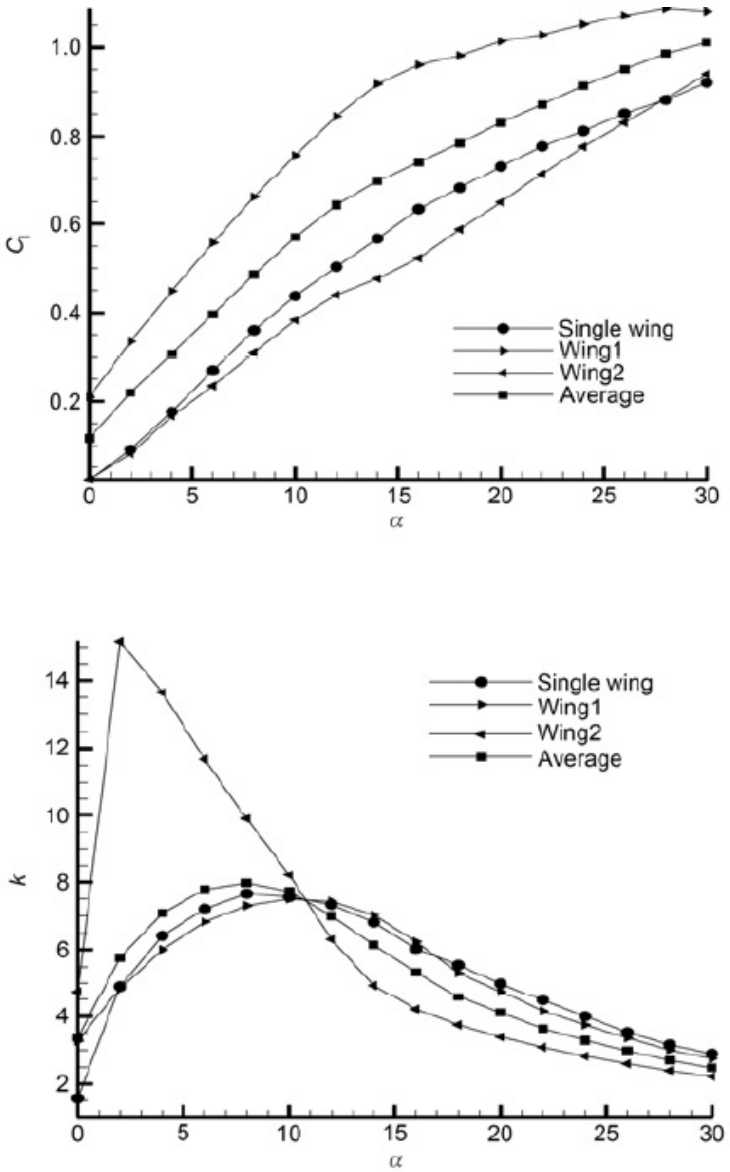

Figure 5.3: Results comparison for the hybrid airship showing lift coefficient versus angle of attack and lift to drag ratio (k) versus angle of attack [28].

Figure 5.4: Piaggio $P180$ Avanti.

5.2 Analytical

5.2.1 The Minimum Induced Drag, Longitudinal Trim and Static Longitudinal Stability of Two-Surface and Three-Surface Airplanes

Combining Prandtl's, Munk's and Laitone's works [29], Eric R. Kendall [30] applies an analytical method in the study of the reduction of induced drag in two and three-surface airplanes (using six different gap configurations, Fig. 5.5) in relation to their change longitudinal trim and static longitudinal stability.

5.2.1.1 Method

The method presented consists of calculating the minimum induced drag (and its penalties) and static longitudinal stability, for both two and three surface configurations, following Prandtl's work on multi planes. The aim of the paper is to determine the surface loading conditions, which produce minimum induced drag on a modern three-surface configuration like the Piaggio $P - 180$ Avanti (Fig. 5.4).

5.2.1.2 Results

The method is then put to the test through some numerical examples, which brings the author to come to the conclusion that the three surface airplane can attain minimum induced drag without compromising the conditions for longitudinal trim and static stability over a useful range of centre of gravity locations . This is in

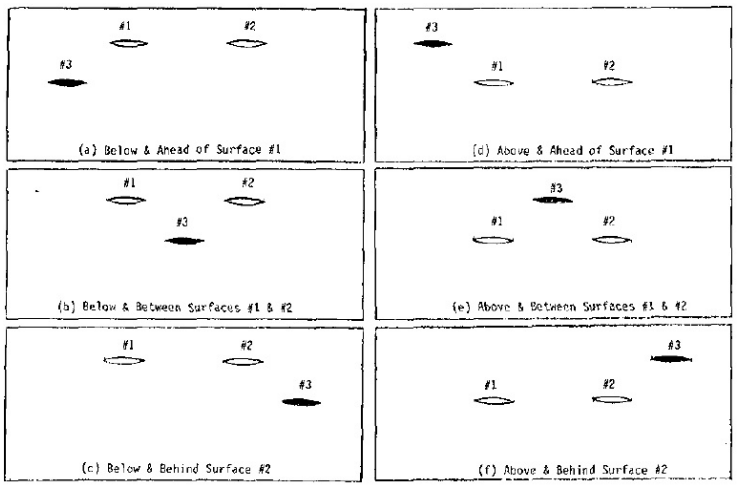

Figure 5.5: The six different gap configurations used by Kendall [30].

favourable comparison with two surface configurations for which longitudinal trim and minimum induced drag can be attained at only one centre of gravity location (hence proving Prandtl's theory of more wings the better).

5.2.2 Subsonic VSTOL Aircraft Configurations with Tandem Wings

Another analytical method obtained through the work of Prandtl and Munk was presented by Julian Wolkovitch [31] for the development of a subsonic VSTOL aircraft. Wolkovitch studies the possibility of using a tandem configuration for such an aircraft, using analytical expressions, and comparing results to wind tunnel test findings, to evaluate the craft's induced drag in contrast to the change of its directional stability and stall characteristics.

5.2.2.1 Method

Similar to what Kendall did in the previous paper presented, the method adopted follows the Prandtl-Munk theory of multi plane aircraft. The method was verified by comparing its results to that of the Vought tandem wing configuration (Fig. 5.6) wind tunnel tests. This sets the basis for a tandem wing-monoplane configuration comparison (Fig. 5.7).

5.2.2.2 Results

The author's conclusions conclusions state that:

1. The Prandtl-Munk theory predicts substantial savings in induced drag for configurations with wings of approximately equal spans having a large gap

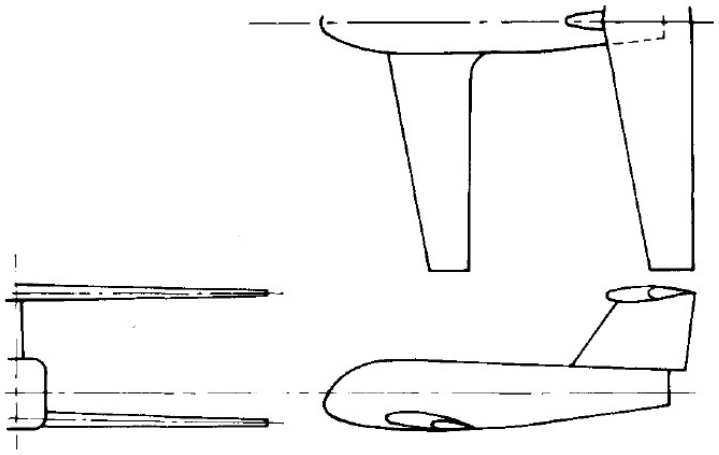

Figure 5.6: Vought tandem wing research model [31].

between the wings. Wind tunnel test data show that the measured induced drag of such configurations is less than the theoretically predicted induced drag (Fig. 5.8).

2. Some configurations which exploit the above mentioned induced-drag advantage have cruise performance superior to conventional designs. One example, presented here, employs tandem wings with the rear wing having gull-type dihedral to provide a large gap at the tips, plus winglets which also act as vertical tails.

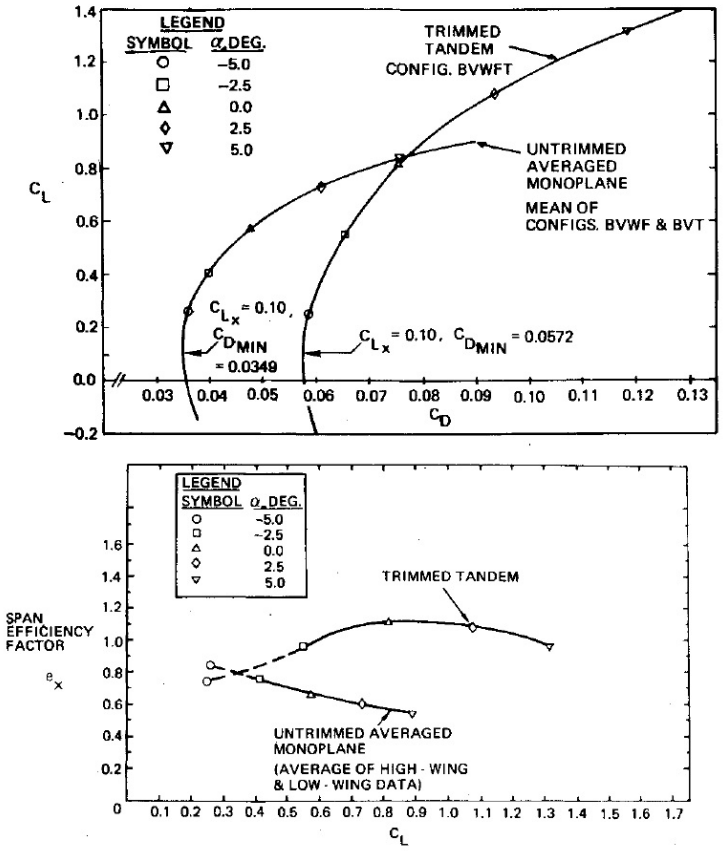

Figure 5.7: Drag polars and span efficiency factors for both tandem wing and monoplane configurations [31].

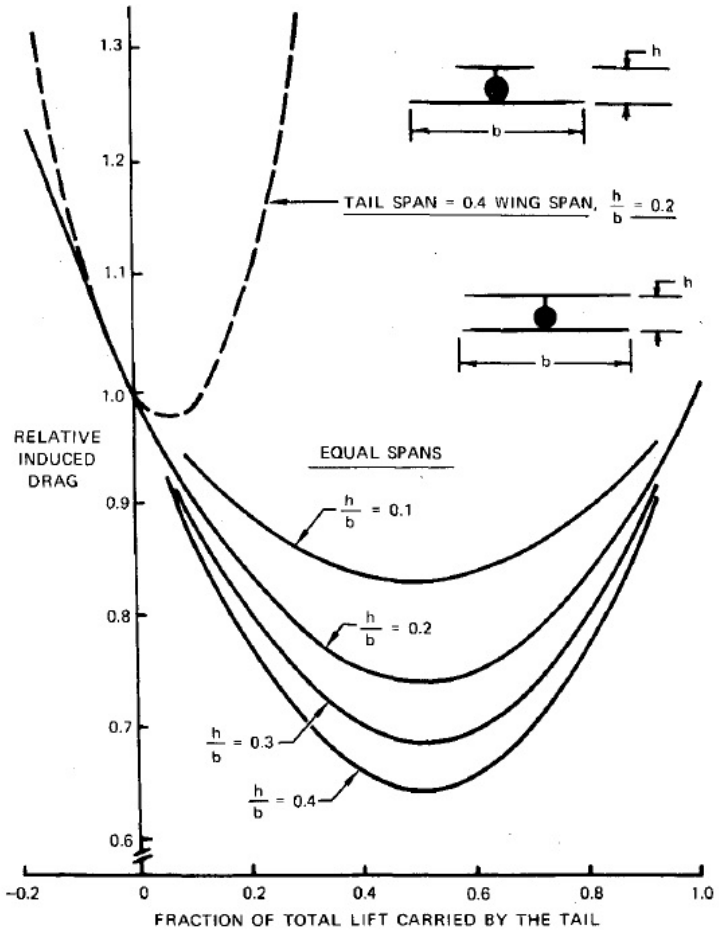

Figure 5.8: Induced drag for tandem wing and conventional wing tail arrangements with optimal span loadings [31].

Part IV

Simplified Computational Scheme

Tandem Wing Model

This part of the work, will present an attempt to model the flight characteristics of the tandem wing configuration. First part of this model, is based on the literature presented specifically for preliminary aircraft design, while the rest of the model has been adapted from flight mechanics models, in order to best describe the physics of the tandem wing configuration. This will concern lift, drag, and pitching moment. No study of the configuration's dynamic stability was made.

The end of this part, will include a collection of results of the model presented, run with data collected from one of the articles described in part III in an attempt to validate the model itself.

Chapter 6

Aircraft Lift, Drag, and Pitching Moment Coefficient

6.1 Lift Curve Slope

Following the work presented by Dr. Jan Roskam in [38], the aircraft's wing lift curve slope may be estimated as:

$$C_{L_{\alpha_w}} = \frac{2\pi A}{\left(2 + \sqrt{\left(\frac{A^2\beta^2}{k^2}\right)\left(1 + \frac{\tan^2 \Lambda_{c/2}}{\beta^2}\right) + 4}\right)} \tag{6.1}$$

where:

$$A = \frac{b^2}{S} \tag{6.2}$$

$$\beta = \sqrt{(1 - M^2)} \tag{6.3}$$

$$k = \frac{(C_{l_\alpha})_{at\,M}}{2\pi} \tag{6.4}$$

and $\Lambda_{c/2}$ represents the semi-chord sweep angle. The airfoil lift curve slope at M in a subsonic case can be estimated as:

$$(C_{l_\alpha})_{at\,M} = \frac{(C_{l_\alpha})_{at\,M=0}}{\left(\sqrt{1 - M^2}\right)} \tag{6.5}$$

the wing-fuselage (or wing-body) lift curve slope is given by:

$$C_{L_{\alpha_{wb}}} = K_{wb} C_{L_{\alpha_w}} \equiv a \tag{6.6}$$

where K_{wb} is the wing-fuselage (or wing body) interference factor given by:

$$K_{wb} = 1 + 0.025\left(\frac{d_f}{b}\right) - 0.25\left(\frac{d_f}{b}\right)^2 \tag{6.7}$$

and d_f is the equivalent fuselage diameter. For future reference the lift curve slope will be referred to as a^w for the aircraft's forward wing and a^p for the aircraft's rearward wing (reference wing and secondary plane respectively).

6.2 Parasite Drag (Zero Lift)

Daniel P. Raymer in [39], presents a simple but effective method of estimating an aircraft's parasite drag or zero lift drag, C_{D_0}. This method is the so called "component build up method", where the zero lift drag is calculated through a collection of specific coefficients each defined for every component of the aircraft. The different component factors are:

- Flat-plate skin-friction drag coefficient, C_f. The flat-plate skin friction coefficient depends upon the Reynolds number, Mach number, and skin roughness. The most important factor affecting skin-friction drag is the extent to which the aircraft has laminar flow over its surfaces:

$$C_f = \frac{0.455}{\left(\log_{10} Re\right)^{2.58} \left(1 + 0.144M^2\right)^{0.65}} \tag{6.8}$$

- Form factor, FF. Different for the type of component :

  Wing, tail, strut, and pylon:

$$FF = \left(1 + \frac{0.6}{(x/c)_m}\left(\frac{t}{c}\right) + 100\left(\frac{t}{c}\right)^4\right)\left(1.34M^{0.18}\left(\cos\Lambda_m\right)^{0.28}\right) \tag{6.9}$$

fuselage and smooth canopy:

$$FF = \left(1 + \frac{60}{f^3} + \frac{f}{400}\right) \tag{6.10}$$

nacelle and smooth external store:

$$FF = 1 + \frac{0.35}{f} \tag{6.11}$$

where:

$$f = \frac{l}{d} = \frac{l}{\sqrt{\frac{4}{\pi}A_{max}}} \tag{6.12}$$

l is the characteristic length chosen, $(x/c)_m$ is the chordwise location of the airfoil maximum thickness point, Λ_m is the sweep angle of the maximum-thickness line.

- Component interference factor, Q. Takes into account that the parasite drag is increased due to the mutual interference between components. For a high-wing, a mid-wing, or a well-fitted low wing, the interference will be negligible so the Q factor will be about 1.0.

Raymer's parasite drag finally reads as:

$$(C_{D_0})_{subsonic} = \frac{\Sigma\left(C_{f_c} FF_c Q_c S_{wet_c}\right)}{S_{ref}} + C_{D_{misc}} + C_{D_{L\&P}} \tag{6.13}$$

where miscellaneous drags, $C_{D_{misc}}$, account for special features of an aircraft such as flaps, unretracted landing gear, an unswept aft fuselage, etc. and leakages and protuberances drags, $C_{D_{L\&P}}$, accounts for the tendency of an aircraft to "inhale" through holes in gaps in high pressure zones and external antennas, lights, etc. respectively.

6.3 Zero Lift Pitching Moment Coefficient

Following the work presented by Dr. Jan Roskam [38] a wing's zero lift pitching moment coefficient (at $M = 0$) may be estimated as:

$$\left(C_{m_{0_w}}\right)_{at\ M=0} = \left(\frac{A\cos^2\Lambda_{c/4}}{A + 2\cos\Lambda_{c/4}}\right)\left(\frac{c_{m_{0_r}} + c_{m_{0_t}}}{2}\right) + \left(\frac{\Delta C_{m_0}}{\epsilon_t}\right)\epsilon_t \tag{6.14}$$

where $c_{m_{0_t}}$ and $c_{m_{0_r}}$, are the zero lift pitching moment coefficients of the root and tip airfoils respectively. $\left(\frac{\Delta C_{m_0}}{\epsilon_t}\right)$ adds a contribution to the zero lift pitching moment coefficient as described by Fig. 6.1.

The generalized wing's zero lift pitching moment coefficient can be described as:

$$\left(C_{m_{0_w}}\right)_{at\ M} = \left(C_{m_{0_w}}\right)_{at\ M=0} \frac{\left(C_{m_0}\right)_M}{\left(C_{m_0}\right)_{M=0}} \tag{6.15}$$

$\frac{\left(C_{m_0}\right)_M}{\left(C_{m_0}\right)_{M=0}}$ can be found from Fig. 6.2.

The wing-fuselage (or wing body) zero lift pitching moment is given by:

$$C_{m_{0_{wb}}} = \left(C_{m_{0_w}} + C_{m_{0_b}}\right)\frac{\left(C_{m_0}\right)_M}{\left(C_{m_0}\right)_{M=0}} \tag{6.16}$$

with:

$$C_{m_{0_b}} = \left(\frac{k_2 - k_1}{36.5S\overline{c}}\right)\left(\Sigma w_{f_i}^2\left(i_w + \alpha_{0_{L_w}} + i_{cl_f}\right)\Delta x_i\right) \tag{6.17}$$

where w_{f_i} and Δx_i are the average width and length of a fuselage segment respectively (Fig. 6.3). $i_w$is the wing incidence angle, $\alpha_{0_{L_w}}$ is the wings zero lift angle of attack, and i_{cl_f} is the incidence angle of the fuselage camber line relative to the fuselage reference plane (Fig. 6.3).

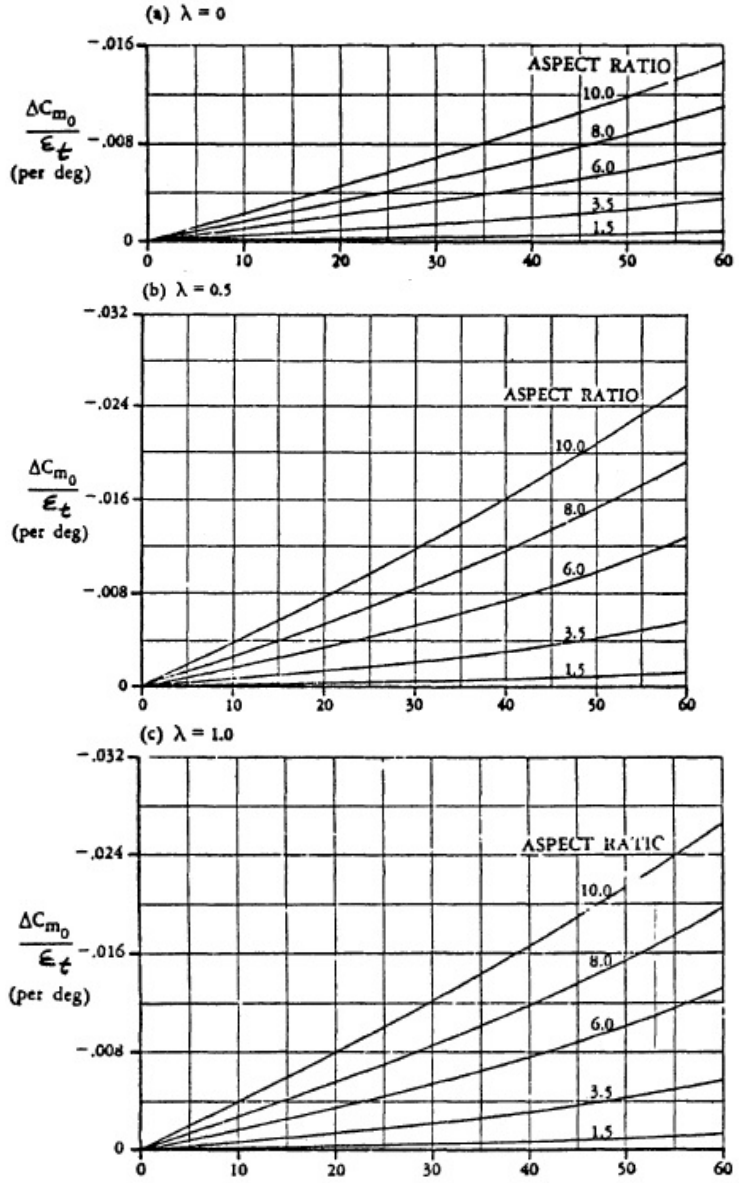

Figure 6.1: Effect of linear twist on wing zero lift pitching moment coefficient.The abscissa for all three planes is the quarter chord sweep angle, $\Lambda_{c/4}$, in degress.

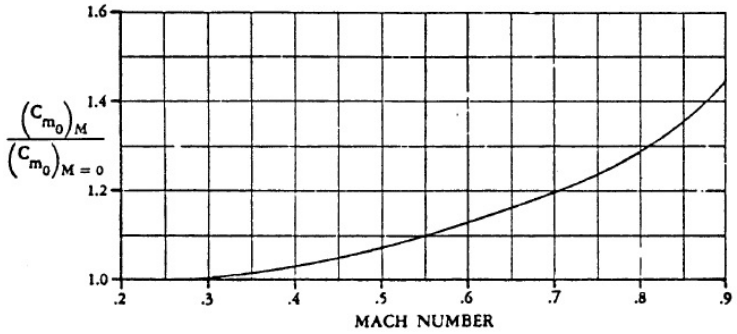

Figure 6.2: Effect of Mach number on wing zero lift pitching moment coefficient.

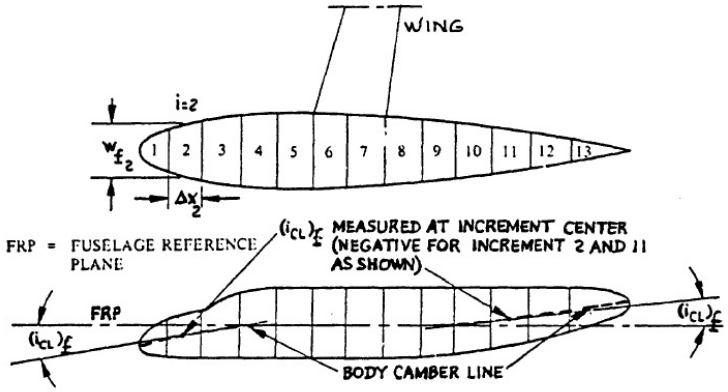

Figure 6.3: Fuselage segmentation and fuselage camber.

Chapter 7

Generalized 2-Surface Configuration

7.1 Lift and Pitching Moment

The lifting system is modelled as the composition of two isolated lifting surfaces, the reference wing (superscript ^{w}) and a secondary plane (superscript ^{p}).There are no a priori assumptions on the placement of the longitudinal control moving surface (elevator).

7.1.1 Reference Wing

The reference wing develops the lift L^w and the pitching moment M^w at its aerodynamic centre A^w:

$$L^w = q_d^w S^w C_L^w \tag{7.1}$$

$$M_{A^w}^w = q_d^w S^w c^w C_{M_{A^w}}^w \tag{7.2}$$

where q^w d is the wing reference dynamic pressure, S^w the wing reference surface, c_w the wing reference chord, C_L^w is the lift coefficient and $C_{M_{A^w}}^w$ the pitching moment coefficient at A^w. The lift coefficient is given by:

$$C_L^w = a^w \alpha^w + b^w \delta \tag{7.3}$$

where α^w is the wing absolute angle of attack, δ the elevator deflection, a^w the lift curve slope with respect to angle of attack and b^w the lift curve slope with respect to elevator deflection. The wing absolute angle of attack is given by:

$$\alpha^w = \alpha + i^w - \epsilon^w(\alpha, \delta) \tag{7.4}$$

where α is the airplane angle of attack, i^w is the wing rigger's incidence (or longitudinal dihedral), and ϵ^w is a perturbation that models the influence of the secondary

plane on the reference wing. We assume that the dependence of this perturbation on (α, δ) is linear:

$$\epsilon^w = \epsilon^w_\alpha \alpha + \epsilon^w_\delta \delta + \epsilon^w_0 \tag{7.5}$$

the pitching moment coefficient at A^w is given by:

$$C^w_{M_{A^w}} \equiv m^w = m^w_0 + m^w_\delta \delta \tag{7.6}$$

where m^w_0 represents its constant part, while m^w_δ ; its moment curve slope with respect to elevator deflection.
Therefore:

$$C^w_L = C^w_{L_\alpha} \alpha + C^w_{L_\delta} \delta + C^w_{L_0} \tag{7.7}$$

$$C^w_{M_{A^w}} = C^w_{M_{A^w_\delta}} \delta + C^w_{M_{A^w_0}} \tag{7.8}$$

with:

$$C^w_{L_\alpha} = (1 - \epsilon^w_\alpha)\, a^w = u^w a^w \tag{7.9}$$

$$C^w_{L_\delta} = (\tau^w - \epsilon^w_\delta)\, a^w = v^w a^w \tag{7.10}$$

$$C^w_{L_0} = (i^w - \epsilon^w_0)\, a^w = j^w a^w \tag{7.11}$$

$$C^w_{M_{A^w{}_\alpha}} = 0 \tag{7.12}$$

$$C^w_{M_{A^w{}_\delta}} = m^w_\delta \tag{7.13}$$

$$C^w_{M_{A^w{}_0}} = m^w_0 \tag{7.14}$$

where τ^w is the ratio:

$$\tau^w = \frac{b^w}{a^w} \tag{7.15}$$

and we have introduced the following quantities:

$$u^w = 1 - \epsilon^w_\alpha \tag{7.16}$$

$$v^w = \tau^w - \epsilon^w_\delta \tag{7.17}$$

$$j^w = i^w - \epsilon^w_0 \tag{7.18}$$

for the sake of brevity.

7.1.2 Secondary Plane

The secondary plane develops the lift L^p and the pitching moment M^p at its aerodynamic centre A^p:

$$L^p = q^p_d S^p C^p_L \tag{7.19}$$

$$M^p_{A^p} = q^p_d S^p c^p C^p_{M_{A^p}} \tag{7.20}$$

where q^p d is the wing reference dynamic pressure, S^p the wing reference surface, c^p the wing reference chord, C^p_L is the lift coefficient and $C^p_{M_{A^p}}$ the pitching moment coefficient at A^p. The lift coefficient is given by:

$$C^p_L = a^p \alpha^p + b^p \delta \tag{7.21}$$

where α^p is the plane absolute angle of attack, a^p the lift curve slope with respect to angle of attack and b^p the lift curve slope with respect to elevator deflection. The plane absolute angle of attack is given by:

$$\alpha^p = \alpha + i^p - \epsilon^p(\alpha, \delta) \tag{7.22}$$

where i^p the plane rigger's incidence (or longitudinal dihedral) and ϵ^p is a perturbation that models the influence of the reference wing on the secondary plane. We assume that the dependence of this perturbation on (α, δ) is linear:

$$\epsilon^p = \epsilon^p_\alpha \alpha + \epsilon^p_\delta \delta + \epsilon^p_0 \tag{7.23}$$

the pitching moment coefficient at A^p is given by:

$$C^p_{M_{A^p}} \equiv m^p = m^p_0 + m^p_\delta \delta \tag{7.24}$$

where m^p_0 represents its constant part, while m^p its moment curve slope with respect to elevator deflection.
Therefore:

$$C^p_L = C^p_{L_\alpha} \alpha + C^p_{L_\delta} \delta + C^p_{L_0} \tag{7.25}$$

$$C^p_{M_{A^p}} = C^p_{M_{A^p_\delta}} \delta + C^p_{M_{A^p_0}} \tag{7.26}$$

with:

$$C^p_{L_\alpha} = (1 - \epsilon^p_\alpha)\, a^p = u^p a^p \tag{7.27}$$

$$C^p_{L_\delta} = (\tau^p - \epsilon^p_\delta)\, a^p = v^p a^p \tag{7.28}$$

$$C^p_{L_0} = (i^p - \epsilon^p_0)\, a^p = j^p a^p \tag{7.29}$$

$$C^p_{M_{A^p_\alpha}} = 0 \tag{7.30}$$

$$C^p_{M_{A^p_\delta}} = m^p_\delta \tag{7.31}$$

$$C^p_{M_{A^p_0}} = m^p_0 \tag{7.32}$$

where τ^p is the ratio:

$$\tau^p = \frac{b^p}{a^p} \tag{7.33}$$

and we have introduced the following quantities:

$$u^p = 1 - \epsilon^p_\alpha \tag{7.34}$$

$$v^p = \tau^p - \epsilon^p_\delta \tag{7.35}$$

$$j^p = i^p - \epsilon^p_0 \tag{7.36}$$

for the sake of brevity.

7.1.3 Complete Airplane

The lift and pitching moment for the complete airplane, under customary hypothesis, are given by:

$$L = L^w + L^p \tag{7.37}$$

$$M_P = M_P^w + M_P^p \tag{7.38}$$

where:

$$M_p^w = M_{A^w}^w - (x_p - x_{A^w})\, L^w \tag{7.39}$$

$$M_P^p = M_{A^p}^p - (x_p - x_{A^p})\, L^p \tag{7.40}$$

the lift and pitching moment coefficients are defined by taking reference on the wing quantities (q_d^w, S^w, c^w), so that:

$$C_L = \frac{1}{q_d^w S^w} = C_L^w + r_q r_S C_L^p \tag{7.41}$$

$$C_{M_P} = \frac{M_p}{q_d^w S^w c^w} = C_{M_P}^w + r_q r_S r_c C_{M_P}^p \tag{7.42}$$

where the following ratios are defined:

$$r_q = \frac{q_d^p}{q_d^w}, \qquad r_S = \frac{S^p}{S^w}, \qquad r_c = \frac{c^p}{c^w} \tag{7.43}$$

and:

$$C_{M_P}^w = m^w - (\xi_P - \xi_{A^w})\, C_L^w \tag{7.44}$$

$$C_{M_P}^p = m^p - \frac{1}{r_c}\,(\xi_P - \xi_{A^p})\, C_L^p \tag{7.45}$$

where $\xi = \frac{x}{c^w}$. Hence:

$$C_L = C_{L_\alpha}\alpha + C_{L_\delta}\delta + C_{L_0} \tag{7.46}$$

$$C_{M_P} = C_{M_{P_\alpha}}\alpha + C_{M_{P_\delta}}\delta + C_{M_{P_0}} \tag{7.47}$$

with:

$$C_{L_\alpha} = (u^w + r u^p)\, a^w \tag{7.48}$$

$$C_{L_\delta} = (v^w + r v^p)\, a^w \tag{7.49}$$

$$C_{L_0} = (j^w + r j^p)\, a^w \tag{7.50}$$

$$C_{M_{P_\alpha}} = (u^w\,(\xi_{A^w} + \xi_P) + r u^p\,(\xi_{A^p} - \xi_P))\, a^w \tag{7.51}$$

$$C_{M_{P_\delta}} = (v^w\,(\xi_{A^w} + \xi_P) + r v^p\,(\xi_{A^p} - \xi_P))\, a^w + (m_\delta^w + \hat{r} m_\delta^p) \tag{7.52}$$

$$C_{M_{P_0}} = ((\xi_{A^w} + \xi_P)\, j^w + (\xi_{A^p} - \xi_P)\, r j^p)\, a^w + (m_0^w + \hat{r} m_0^p) \tag{7.53}$$

with:

$$r_a = \frac{a^p}{a^w}, \qquad r = r_q r_S r_a, \qquad \hat{r} = r_q r_S r_c \tag{7.54}$$

7.2 Constitutive Parameters

7.2.1 Neutral Point

From the general definition of the neutral point N, the following holds:

$$\xi_N = \xi_P + \frac{C_{M_{P_\alpha}}}{C_{L_\alpha}} \tag{7.55}$$

so that:

$$\xi_N = u^w \xi_{A^w} + r u^p \xi_{A^p} = \xi_{A^w} - \frac{r u^p}{u^w + r u^p} \Delta\xi_A \tag{7.56}$$

where:

$$\Delta\xi_A = \xi_{A^w} - \xi_{A^p} \tag{7.57}$$

which represents the stagger between the reference wing and the secondary plane aerodynamic centres.

7.2.2 Control Point

From the general definition for the control point C, the following holds:

$$\xi_C = \xi_P + \frac{C_{M_{P_\delta}}}{C_{L_\delta}} \tag{7.58}$$

so that:

$$\begin{gathered}\xi_C = \frac{(v^w \xi_{A^w} + r v^p \xi_{A^p}) a^w + m_\delta}{(v^w + r v^p) a^w} = \frac{v^w \xi_{A^w} + r v^p \xi_{A^p}}{v^w + r v^p} + \zeta = \\ = \xi_{A^p} + \frac{v^w}{v^w + r v^p} \Delta\xi_A + \zeta\end{gathered} \tag{7.59}$$

where:

$$m_\delta = m_\delta^w + \hat{r} m_\delta^p \tag{7.60}$$

and:

$$\zeta = \frac{m_\delta}{(v^w + r v^p)\, a^w} \tag{7.61}$$

7.2.3 Aerodynamic Length

The airplane non dimensional aerodynamic length is:

$$\begin{gathered}\lambda = \xi_N - \xi_C = \frac{(u^w v^p - u^p v^w) r}{(u^w + r u^p)(v^w + r v^p)} \Delta\xi_A - \zeta = \\ = \frac{wr}{uv} \Delta\xi_A - \zeta\end{gathered} \tag{7.62}$$

having defined:

$$u = u^w + r u^p \tag{7.63}$$

$$v = v^w + r v^p \tag{7.64}$$

$$w = u^w v^p - u^p v^w \tag{7.65}$$

for the sake of brevity.
The characteristic determinant is:

$$\begin{gathered}\Delta = -\lambda C_{L_\alpha} C_{L_\delta} = -\left(\left(u^w v^p - u^p v^w\right) r \Delta\xi_A - \left(u^w + r u^p\right)\left(v^w + r v^p\right)\zeta\right)(a^w)^2 = \\ = -\left(wr\Delta\xi_A - uv\zeta\right)(a^w)^2\end{gathered} \tag{7.66}$$

7.2.4 Zero Lift and Moment Angles

The zero lift and moment angles are defined as:

$$\alpha_0 = \frac{C_{L_\delta} C_{M_{P_0}} - C_{L_0} C_{M_{P_\delta}}}{\Delta} \tag{7.67}$$

$$\delta_0 = \frac{C_{L_0} C_{M_{P_\alpha}} - C_{L_\alpha} C_{M_{P_0}}}{\Delta} \tag{7.68}$$

Therefore:

$$\alpha_0 = j_\alpha - \frac{\mu}{C_{L_\alpha}} \tag{7.69}$$

$$\delta_0 = j_\delta + \frac{\mu}{C_{L_\delta}} \tag{7.70}$$

with:

$$j_\alpha = \frac{j^p v^w - j^w v^p}{w} \tag{7.71}$$

$$j_\delta = \frac{j^w u^p - j^p u^w}{w} \tag{7.72}$$

and:

$$\mu = \frac{1}{\lambda} \left(m_0 + m_\delta j_\delta \right) \tag{7.73}$$

7.3 Trim Characteristics

7.3.1 Trim Solution

At trim, the following general result holds:

$$\alpha - \alpha_0 \left(1 - e\right) \frac{C_L}{C_{L_\alpha}} \tag{7.74}$$

$$\delta - \delta_0 = -e \frac{C_L}{C_{L_\delta}} \tag{7.75}$$

where:

$$e = \frac{\xi_G - \xi_N}{\lambda} \tag{7.76}$$

the previous expressions can be cast as:

$$\alpha = \alpha_1(e) \frac{C_L}{a^w} + \alpha_0 \tag{7.77}$$

$$\delta = \delta_1(e) \frac{C_L}{a^w} + \delta_0 \tag{7.78}$$

where the following coefficients have been defined:

$$\alpha_1(e) = \frac{1 + e}{u} \tag{7.79}$$

$$\delta_1(e) = -\frac{e}{v} \tag{7.80}$$

7.3.2 Trim Values for Lift Coefficients

The lift coefficient of the reference wing reads:

$$C_L^w = a^w \left(u^w \alpha + v^w \delta + j^w\right) = a^w \left(u^w \left(\alpha_1(e)\frac{C_L}{a^w} + \alpha_0\right) + v^w \left(\delta_1(e)\frac{C_L}{a^w} + \delta_0\right) + j^w\right) = \\ = \left(u^w \alpha_1(e) + v^w \delta_1(e)\right) C_L + \left(j^w + u^w \alpha_0 + v^w \delta_0\right) a^w = \\ = \gamma_1^w(e) C_L + \gamma_0^w \tag{7.81}$$

where:

$$\gamma_1^w(e) = \frac{u^w}{u} + e\frac{wr}{uv} = \overline{u}^w + er\overline{w} \tag{7.82}$$

$$\gamma_0^w = -\left(\frac{u^w}{u} + \frac{v^w}{v}\right)\mu = -\left(\overline{u}^w - \overline{v}^w\right)\mu \tag{7.83}$$

with:

$$\overline{u}^w = \frac{u^w}{u}, \qquad \overline{v}^w = \frac{v^w}{v}, \qquad \overline{w} = \frac{w}{uv} \tag{7.84}$$

the lift coefficient of the secondary plane reads:

$$C_L^p = a^p \left(u^p \alpha + v^p \delta + j^p\right) = a^p \left(u^p \left(\alpha_1(e)\frac{C_L}{a^w} + \alpha_0\right) + v^p \left(\delta_1(e)\frac{C_L}{a^w} + \delta_0\right) + j^p\right) = \\ = r_a \left(\left(u^p \alpha_1(e) + v^p \delta_1(e)\right) C_L + \left(j^p + u^p \alpha_0 + v^p \delta_0\right) a^w\right) = \\ = r_a \left(\gamma_1^p(e) C_L + \gamma_0^p\right) \tag{7.85}$$

where:

$$\gamma_1^p(e) = \frac{u^p}{u} - e\frac{w}{uv} = \overline{u}^p - e\overline{w} \tag{7.86}$$

$$\gamma_0^p = -\left(\frac{u^p}{u} - \frac{v^p}{v}\right)\mu = -\left(\overline{u}^p - \overline{v}^p\right)\mu \tag{7.87}$$

with:

$$\overline{u}^p = \frac{u^p}{u}, \qquad \overline{v}^p = \frac{v^p}{v} \tag{7.88}$$

7.3.3 Trim Functions for Drag Coefficients

We assume an ideal analytic polar for the reference wing:

$$C_D^w = C_{D_0}^w + K^w C_L^{w2} \tag{7.89}$$

so that, by substituting the trim value for C_L^w, we get:

$$C_D^w = C_{D_0}^w + K^w \left(\gamma_1^w C_L + \gamma_0^w\right)^2 = C_{D_0}^w + K^w \gamma_0^{w^2} + 2K^w \gamma_0^w \gamma_1^w C_L + K^w \gamma_1^{w^2} C_L^2 = \\ = \omega_0^w + \omega_1^w(e) C_L + \omega_2^w(e) C_L^2 \tag{7.90}$$

´with:

$$\omega_0^w = C_{D_0}^w + K^w \gamma_0^{w2} = C_{D_0}^w + K^w \left(\overline{u}^w - \overline{v}^w\right)^2 \mu^2 \tag{7.91}$$

$$\omega_1^w(e) = 2K^w \gamma_0^w \gamma_1^w(e) = -2K^w \left(\overline{u}^w - \overline{v}^w\right)\left(\overline{u}^w + er\overline{w}\right)\mu \tag{7.92}$$

$$\omega_2^w(e) = K^w \gamma_1^w(e)^2 = K^w \left(\overline{u}^w + er\overline{w}\right)^2 \tag{7.93}$$

we assume an ideal analytic polar for the secondary plane:

$$C_D^p = C_{D_0}^p + K^p C_L^{p^2} \tag{7.94}$$

so that, by substituting the trim value for C_L^w, we get:

$$C_D^p = C_{D_0}^p + K^p r_a^2 \left(\gamma_1^p C_L + \gamma_0^p\right)^2 = C_{D_0}^p + K^p r_a^2 \gamma_0^{p^2} + 2K^p r_a^2 \gamma_0^p \gamma_1^p C_L + K^p r_a^2 \gamma_1^{p^2} C_L^2 = \\ = \omega_0^p + \omega_1^p(e) C_L + \omega_2^p(e) C_L^2 \tag{7.95}$$

with:

$$\omega_0^p = C_{D_0}^p + K^p r_a^2 \gamma_0^{p^2} = C_{D_0}^p + K^p r_a^2 \left(\overline{u}^p - \overline{v}^p\right)^2 \mu^2 \tag{7.96}$$

$$\omega_1^p(e) = 2K^p r_a^2 \gamma_0^p \gamma_1^p(e) = -2K^p r_a^2 \left(\overline{u}^p - \overline{v}^p\right)\left(\overline{u}^p + e\overline{w}\right)\mu \tag{7.97}$$

$$\omega_2^p(e) = K^p r_a^2 \gamma_1^p(e)^2 = K^p r_a^2 \left(\overline{u}^p + e\overline{w}\right)^2 \tag{7.98}$$

7.3.4 Trimmed Polar Curve

The drag for the complete airplane, under customary hypothesis is given by:

$$D = D^w + D^p \tag{7.99}$$

so that:

$$C_D = C_D^w + r_q r_S C_D^p \tag{7.100}$$

as a result, the trim function of the complete airplane drag coefficient (trimmed polar curve) is given by:

$$C_D = C_{D_0} + H(e) C_L + K(e) C_L^2 \tag{7.101}$$

where:

$$C_{D_0} = \omega_0^w + r_q r_S \omega_0^p \tag{7.102}$$

$$H(e) = \omega_1^w(e) + r_q r_S \omega_1^p(e) \tag{7.103}$$

$$K(e) = \omega_2^w(e) + r_q r_S \omega_2^p(e) \tag{7.104}$$

or:

$$C_{D_0} = \left(1 + r_q r_S r_D\right) C_{D_0}^w + \left(\left(\overline{u}^w - \overline{v}^w\right)^2 + r r_a r_K \left(\overline{u}^p - \overline{v}^p\right)^2\right) K^w \mu^2 \tag{7.105}$$

$$H(e) = -2\left(\left(\overline{u}^w - \overline{v}^w\right)\left(\overline{u}^w + er\overline{w}\right) + r r_a r_K \left(\overline{u}^p - \overline{v}^p\right)\left(\overline{u}^p - e\overline{w}\right)\right) K^w \mu \tag{7.106}$$

$$K(e) = \left(\left(\overline{u}^w + er\overline{w}\right)^2 + r r_a r_K \left(\overline{u}^p - e\overline{w}\right)^2\right) K^w \tag{7.107}$$

having defined the following ratios:

$$r_D = \frac{C_{D_0}^p}{C_{D_0}^w}, \qquad r_K = \frac{K^p}{K^w} \tag{7.108}$$

possible more compact expressions are:

$$C_{D_0} = \left(1 + \tilde{r}\right) C_{D_0}^w + \left(\overline{y}^{w^2} + \check{r}\overline{y}^{p^2}\right) K^w \mu^2 \tag{7.109}$$

$$H = -2\left(\overline{y}^w \overline{z}^w + \check{r}\overline{y}^p \overline{z}^p\right) K^w \mu \tag{7.110}$$

$$K = \left(\overline{z}^{w^2} + \check{r}\overline{z}^{p^2}\right) K^w \tag{7.111}$$

where:

$$\tilde{r} = r_q r_S r_D, \qquad \check{r} = r r_a r_K \tag{7.112}$$

$$\overline{y}^w = \overline{u}^w - \overline{v}^w, \qquad \overline{y}^p = \overline{u}^p - \overline{v}^p \tag{7.113}$$

$$\overline{z}^w(e) = \overline{u}^w + er\overline{w}, \qquad \overline{z}^p(e) = \overline{u}^p + e\overline{w} \tag{7.114}$$

7.4 Typical Tail-Aft Airplane

7.4.1 Interaction Model

For a typical tail-aft airplane, the reference wing is the wing-body assembly and the secondary plane is the horizontal tailplane located after the wing. We assume that

1. The longitudinal control moving surface (elevator) lies on the horizontal tailplane;
2. The wing and horizontal tailplane are separated enough to make the influence of the latter on the former negligible.

By assumption 1, we get:

$$b^w = 0 \tag{7.115}$$

$$m_\delta^w = 0 \tag{7.116}$$

and by assumption 2,

$$\epsilon_\alpha^w = \epsilon_\delta^w = \epsilon_0^w = 0 \tag{7.117}$$

for the horizontal tailplane, we get:

$$\epsilon^p = \epsilon_\alpha^p \alpha + \epsilon_0^p \tag{7.118}$$

and, since $\epsilon^p = 0$ when $C_L^w = 0$, we have:

$$\epsilon_0^p = \epsilon_\alpha^p i^w \tag{7.119}$$

7.4.2 Lift and Pitching Moment

Given the above expressions, we get:

$$u^w = 1, \qquad u^p = 1 - \epsilon_\alpha^p \tag{7.120}$$

$$v^w = 0, \qquad v^p = \tau^p \tag{7.121}$$

$$j^w = i^w, \qquad j^p = i^p - \epsilon_\alpha^p i^w \tag{7.122}$$

so that:

$$C_{L_\alpha} = (1 + r u^p)\, a^w \tag{7.123}$$

$$C_{L_\delta} = r \tau^p a^w \tag{7.124}$$

$$C_{L_0} = (i^w + r j^p)\, a^w \tag{7.125}$$

$$C_{M_{P_\alpha}} = ((\xi_{A^w} + \xi_P)\, r u^p\, (\xi_{A^p} - \xi_P))\, a^w \tag{7.126}$$

$$C_{M_{P_\delta}} = r \tau^p\, (\xi_{A^p} - \xi_P)\, a^w + \hat{r} m_\delta^w \tag{7.127}$$

$$C_{M_{P_0}} = ((\xi_{A^w} - \xi_P)\, i^w + (\xi_{A^p} - \xi_P)\, r j^p)\, a^w + (m_0^w + \hat{r} m_0^p) \tag{7.128}$$

7.4.3 Characteristic Points

The neutral and control point positions read

$$\xi_N = \frac{\xi_{A^w} + ru^p \xi_{A^p}}{1 + ru^p} = \frac{\xi_{A^w} + (1-u)\,\xi_{A^p}}{u} \tag{7.129}$$

$$\xi_C = \xi_{A^p} + \zeta \tag{7.130}$$

where:

$$\zeta = \frac{\hat{r}}{r}\frac{m_\delta^p}{v^p a^w} = \frac{r_c}{r_a}\frac{m_\delta^p}{\tau^p a^w} \tag{7.131}$$

the airplane non dimensional aerodynamic length is:

$$\lambda = \frac{1}{1 + ru^p}\Delta\xi_A - \zeta \tag{7.132}$$

since:

$$u = 1 + ru^p, \qquad v = rv^p, \qquad w = v^p \tag{7.133}$$

the characteristic determinant is:

$$\Delta = -\left(\Delta\xi_A - (1 + ru^p)\,\zeta\right) r v^p {a^w}^2 = -\left(\Delta\xi_A - u\zeta\right) r\tau^p {a^w}^2 \tag{7.134}$$

7.4.4 Zero Lift and Moment Angles

The zero lift and moment angles are:

$$\alpha_0 = -i^w - \frac{\mu}{C_{L_\alpha}} \tag{7.135}$$

$$\delta_0 = \frac{\Delta i}{\tau^p} + \frac{\mu}{C_{L_\delta}} \tag{7.136}$$

since:

$$j_\alpha = -\frac{i^w v^p}{w} = -i^w \tag{7.137}$$

$$j_\delta = \frac{j^w u^p - j^p}{w} = \frac{\Delta i}{\tau^p} \tag{7.138}$$

with:

$$\Delta i = i^w - i^p \tag{7.139}$$

and:

$$\mu = \frac{1}{\lambda}\left(m_0^w + \hat{r}\left(m_0^p + m_\delta^p \frac{\Delta i}{\tau^p}\right)\right) \tag{7.140}$$

7.4.5 Trim Values for Lift Coefficients

The lift coefficient of the wing-body reads:

$$C_L^w = \gamma_1^w(e) C_L + \gamma_0^w \tag{7.141}$$

where:

$$\gamma_1^w(e) = \frac{1+e}{u} \tag{7.142}$$

$$\gamma_0^w = -\frac{\mu}{u} \tag{7.143}$$

since:

$$\overline{u}^w = \frac{1}{u}, \qquad \overline{v}^w = 0, \qquad \overline{w} = \frac{1}{u} \tag{7.144}$$

the lift coefficient of the horizontal tailplane reads:

$$C_L^p = r_a \left(\gamma_1^p(e) C_L + \gamma_0^p\right) \tag{7.145}$$

where:

$$\gamma_1^p(e) = \frac{u^p - e}{u} \tag{7.146}$$

$$\gamma_0^p = -\frac{1}{r}\frac{\mu}{u} \tag{7.147}$$

since:

$$\overline{u}^p = \frac{u^p}{u}, \qquad \overline{v}^p = \frac{1}{r} \tag{7.148}$$

7.4.6 Trim Functions for Drag Coefficients

The trimmed polar for the wing-body reads:

$$C_D^w = \omega_0^w + \omega_1^w(e) C_L + \omega_2^w(e) C_L^2 \tag{7.149}$$

with:

$$\omega_0^w = C_{D_0}^w + \frac{K^w}{u^2}\mu^2 \tag{7.150}$$

$$\omega_1^w(e) = -2\left(1+e\right)\frac{K^w}{u^2}\mu \tag{7.151}$$

$$\omega_2^w(e) = \left(1+e\right)^2 \frac{K^w}{u^2} \tag{7.152}$$

the trimmed polar for the horizontal tailplane reads:

$$C_D^p = \omega_0^p + \omega_1^p(e) C_L + \omega_2^p(e) C_L^2 \tag{7.153}$$

with:

$$\omega_0^p = C_{D_0}^p + \frac{r_a^2}{r^2}\frac{K^p}{u^2}\mu^2 \tag{7.154}$$

$$\omega_1^p(e) = -2 f(e) \frac{r_a^2}{r^2}\frac{K^p}{u^2}\mu \tag{7.155}$$

$$\omega_2^p(e) = f(e)^2 \frac{r_a^2}{r^2}\frac{K^p}{u^2} \tag{7.156}$$

with:

$$f(e) = e - \left(1-e\right) r u^p \tag{7.157}$$

7.4.7 Trimmed Polar Curve

The trim function of the complete airplane drag coefficient (trimmed polar curve) is given by:

$$C_D = C_{D_0} + H(e)C_L + K(e)C_L^2 \tag{7.158}$$

where:

$$C_{D_0} = (1+\tilde{r})\, C_{D_0}^w + (1+k)\, \frac{K^w}{u^2}\mu^2 \tag{7.159}$$

$$H(e) = -2\left((1+e) + sf(e)\right)\frac{K^w}{u^2}\mu \tag{7.160}$$

$$K(e) = \left((1+e)^2 + sf(e)^2\right)\frac{K^w}{u^2} \tag{7.161}$$

having defined:

$$s = \frac{r_K r_a}{r} \equiv \frac{r_K}{r_q r_S} \tag{7.162}$$

for the sake of brevity.
Also, with reference to the minimum drag coefficient C_{D_m}, achieved for $C_L = C_{L_m}$, we get:

$$C_D = C_{D_m}(e) + K(e)\left(C_L - C_{L_m}\right)^2 \tag{7.163}$$

where:

$$C_{L_m}(e) = -\frac{H(e)}{K(e)} \tag{7.164}$$

$$C_{D_m}(e) = C_{D_0} - K(e)C_{L_m}(e)^2 = C_{D_0} - \frac{H(e)^2}{K(e)} \tag{7.165}$$

therefore:

$$C_{L_m}(e) = 2\frac{(1+e) + sf(e)}{(1+e)^2\, sf(e)^2}\mu \tag{7.166}$$

$$C_{D_m}(e) = (1+\tilde{r})\, C_{D_0}^w + \left((1+s) - 4\frac{\left((1+e)\, sf(e)\right)^2}{(1+e)^2 + sf(e)^2}\right)\frac{K^w}{u^2}\mu^2 \tag{7.167}$$

7.5 Tandem Wing Airplane

For a canard-type tandem wing airplane, the reference wing is the rearward wing-body assembly and the secondary plane is the forward wing. We assume that the longitudinal control moving surface (elevator) lies on the forward wing (canard-type).

By assumption such assumption, we get:

$$b^w = 0 \tag{7.168}$$

$$m_\delta^w = 0 \tag{7.169}$$

Closely-coupled system The case for a closely coupled tandem wing system, i.e. when both the influence of the forward wing on the rearward wing, and that of the rearward wing on the forward wing, amounts to the general case - taking into account the previous simplifications for b^w and m_δ^w.

Loosely-coupled system The case for a loosely coupled tandem wing system is given when some part of the influence of one wing upon the other is negligible. For example, this may be the case when the forward wing is lower than the upward wing, with suitable gap and stagger, so that the downwash of the forward wing is hardly felt on the rearward wing, while the upwash of the rearward wing does influence the aerodynamics of the forward wing.

Therefore, in this case, we get:

$$\epsilon_\alpha^w = \epsilon_\delta^w = \epsilon_0^w = 0 \tag{7.170}$$

$$\epsilon^p = \epsilon_\alpha^p \alpha + \epsilon_0^p \tag{7.171}$$

and since $\epsilon^p = 0$ when $C_L^w = 0$, we have:

$$\epsilon_0^p = \epsilon_\alpha^p i^w \tag{7.172}$$

Therefore, this case formally coincides with that of the typical tail-aft airplane.

Uncoupled system The case for an uncoupled tandem wing system is given when the arrangement, gap and stagger are such that no influence of one wing is felt on the other.

In this case:

$$\epsilon_\alpha^w = \epsilon_\delta^w = \epsilon_0^w = 0 \tag{7.173}$$

$$\epsilon_\alpha^p = \epsilon_\delta^p = \epsilon_0^p = 0 \tag{7.174}$$

given the above, we get:

$$u^w = 1, \qquad u^p = 1 \tag{7.175}$$

$$v^w = 0, \qquad v^p = \tau^p \tag{7.176}$$

$$j^w = i^w, \qquad j^p = i^p \tag{7.177}$$

so that:

$$C_{L_\alpha} = (1 + r)\, a^w \tag{7.178}$$

$$C_{L_\delta} = r\tau^p a^w \tag{7.179}$$

$$C_{L_0} = (i^w + r i^p)\, a^w \tag{7.180}$$

$$C_{M_{P_\alpha}} = ((\xi_{A^w} + \xi_P) + r\,(\xi_{A^p} - \xi_P))\, a^w \tag{7.181}$$

$$C_{M_{P_\delta}} = r\tau^p\,(\xi_{A^p} - \xi_P)\, a^w + \hat{r} m_\delta^w \tag{7.182}$$

$$C_{M_{P_0}} = ((\xi_{A^w} + \xi_P)\, i^w + (\xi_{A^p} - \xi_P)\, r i^p)\, a^w + (m_0^w + \hat{r} m_0^p) \tag{7.183}$$

therefore:

$$\xi_N = \frac{\xi_{A^w} + r\xi_{A^p}}{1 + r u^p} \tag{7.184}$$

$$\xi_C = \xi_{A^p} + \zeta \tag{7.185}$$

$$\lambda = \frac{1}{1+r}\Delta\xi_A - \zeta \tag{7.186}$$

$$\Delta = -\left(\Delta\xi_A - (1+r)\,\zeta\right) r v^p a^{w^2} \tag{7.187}$$

$$\alpha_0 = -i^w - \frac{\mu}{C_{L_\alpha}} \tag{7.188}$$

$$\delta_0 = \frac{\Delta i}{\tau^p} + \frac{\mu}{C_{L_\delta}} \tag{7.189}$$

$$\gamma_1^w(e) = \frac{1+e}{1+r} \tag{7.190}$$

$$\gamma_0^w = -\frac{\mu}{1+r} \tag{7.191}$$

$$\gamma_1^p(e) = \frac{1-e}{1+r} \tag{7.192}$$

$$\gamma_0^p = -\frac{1}{r}\frac{\mu}{1+r} \tag{7.193}$$

Chapter 8

Results

In order to validate the presented method, a verification of its hypothesised approach was carried out. This was done through a simple comparison with the work presented by Olson and Selberg and their $3D$ test and results on a biplane and fuselage test model (Fig. 8.1). The first step was to was to calculate the needed data in chapter 6 and then run the uncoupled $2-$surface method with such data.

8.1 Initial Data

There are two separate sets of initial data. One that comes from the article itself, which include the dimensions of the model tested, the test matrix, and the type of airfoil. The second set is related to the type of airfoil itself, as the initial data needed to calculate what was presented in chapter 6, is not given in the article itself, this data was calculated through the use of a panel method software.

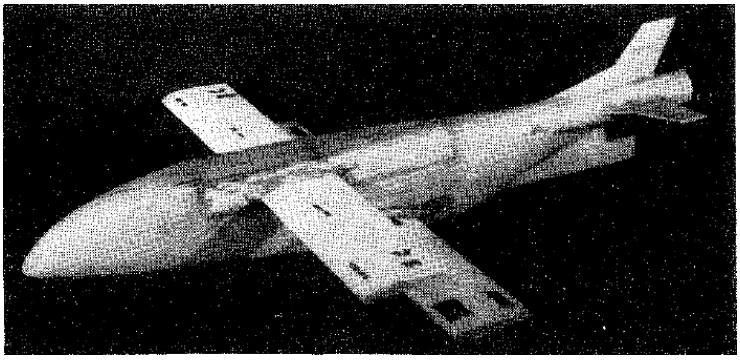

Figure 8.1: Fuselage with biplane wing system test model.

Data	Value	Unit
Reynolds Number	2.871×10^5	adim.
Chord (c)	0.100	m
Span (b)	1.244	m
Wing area (S)	0.126	m^2
Fuselage diameter (d_f)	0.311	m
Fuselage length (l)	1.400	m
Taper ratio (λ)	-	adim.
Airfoil type	$NACA\ 2412$	-

Table 8.1: Initial data presented.

Data	Value	Unit
Lift curve slope (C_{l_α})	6.075	rad^{-1}
Zero lift pitching moment coefficient (c_{m_0})	-0.062	adim.

Table 8.2: Initial data calculated with *XFoil*.

Olson and Selberg Data

The initial data presented in the article is hereby summarised in Tab. 8.1. All values shown have been converted to SI units, while the paper presents them in $Imperial\,Units$ system.

Airfoil Data

Through the use of a panel method software (*XFoil*), the data presented in Tab. 8.2 was calculated for the $NACA\ 2412$ airfoil. These values are then used to calculate the wing-body lift curve slope and zero lift pitching moment, as described in sections 6.1 and 6.2 respectively.

8.2 Data Rebuild

The first goal of the method is to compare lift curve slopes between the experimental data from Olson's and Selberg's work, and the $2-$surface method presented. Since the paper does not present a lift curve slope directly, this had to be built from a simple interpolation of two curves.

Using the results presented from the efficiency versus lift coefficient curve, and the drag coefficient versus angle of attack curve. Data used is hereby presented.

Interpolation

Both the efficiency versus lift coefficient curve, and the drag coefficient versus angle of attack curve, have been reproduced from the original paper in order to obtain the full range of values need for the interpolation. These reconstructions can be

seen in Fig. 8.2. This all results in the lift curve slope shown in Fig. 8.3 for the two decalage angles used in the paper presented.

Discretisation

Clearly the most interesting part of the interpolation, is the linear section, between 5° and 12° approximately. Hence the lift curve slope created, was descritised, as can be seen in Fig. 8.4.

8.3 2-Surface Method: Uncoupled System

To first apply the method described in chapter 7, the uncoupled system was chosen as a first base of trials and tests to be run on the given data. The uncoupled tandem wing system defines the arrangement, gap and stagger as having no influence on one wing over the other. Hence sets an ideal starting point.

This means that:

$$\begin{aligned} \epsilon_\alpha^w = \epsilon_\delta^w = \epsilon_0^w = 0 \\ \epsilon_\alpha^p = \epsilon_\delta^p = \epsilon_0^p = 0 \end{aligned} \tag{8.1}$$

Results found are shown in Fig. 8.5.

8.4 Experimental Versus Uncoupled System

Fig. 8.6 shows the comparison between the results obtained by Olson and Selberg, and the uncoupled system results (with downwash set to zero). The next section will concentrate on trying to find the right value of downwash, which will allow the two results obtain to match as much as possible.

8.5 Experimental Versus Closely-Coupled System

The next step was to introduce a downwash value (closely-coupled system described in section 7.5), which allowed the uncoupled system curve to mimic the experimental curve, at least in its central linear part, as best as possible. The closely-coupled system results can be seen in Fig. 8.7. These graphs show how at a constant downwash value, the change in decalage angle, changes the lift curve slope quite evidently. This goes to show that a downwash model, with a dependence on (α, δ) only, is not sufficient to fully describe the tandem wing configuration.

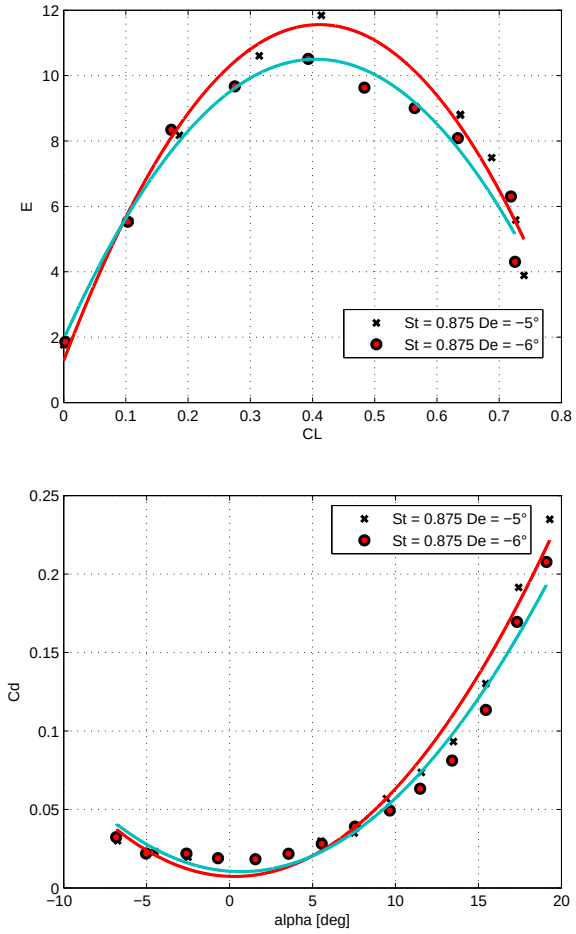

Figure 8.2: Reconstructed efficiency versus lift coefficient curve (top), and Reconstructed drag coefficient versus angle of attack cruve.

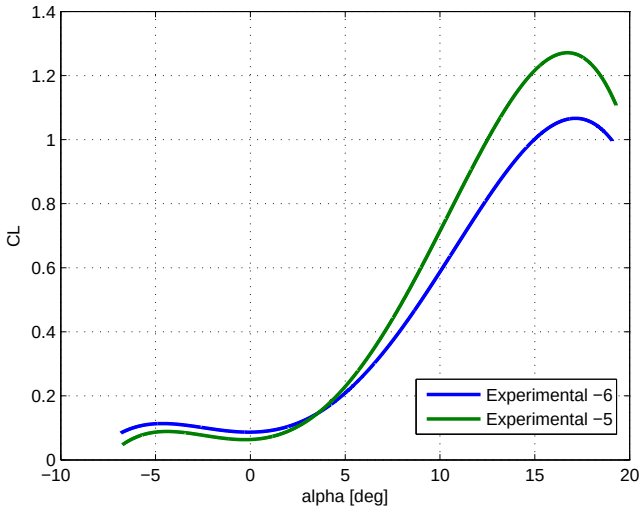

Figure 8.3: Interpolated lift coefficient versus angle of attack curve.

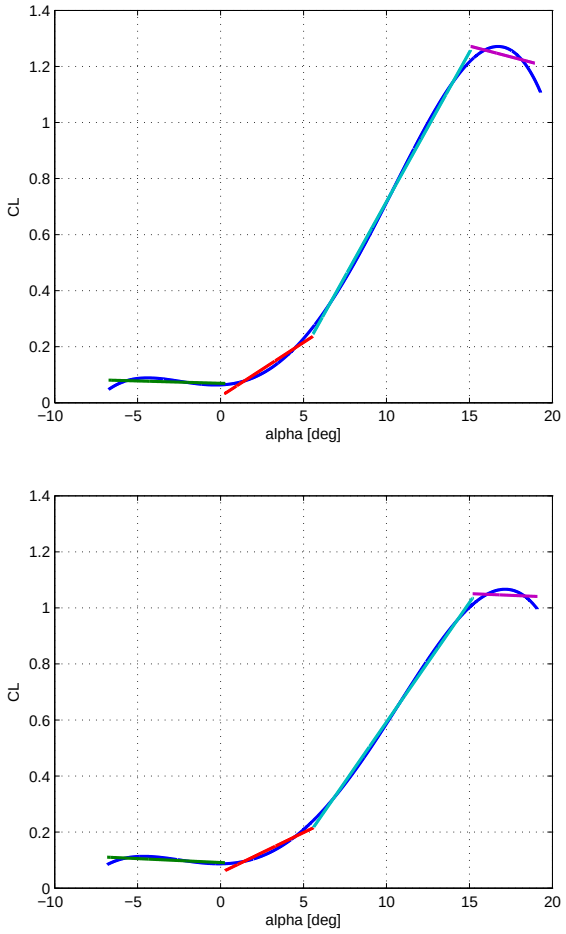

Figure 8.4: Descritized lift curve slope at $De = -5°$ (top), and $De = -6°$ (bottom).

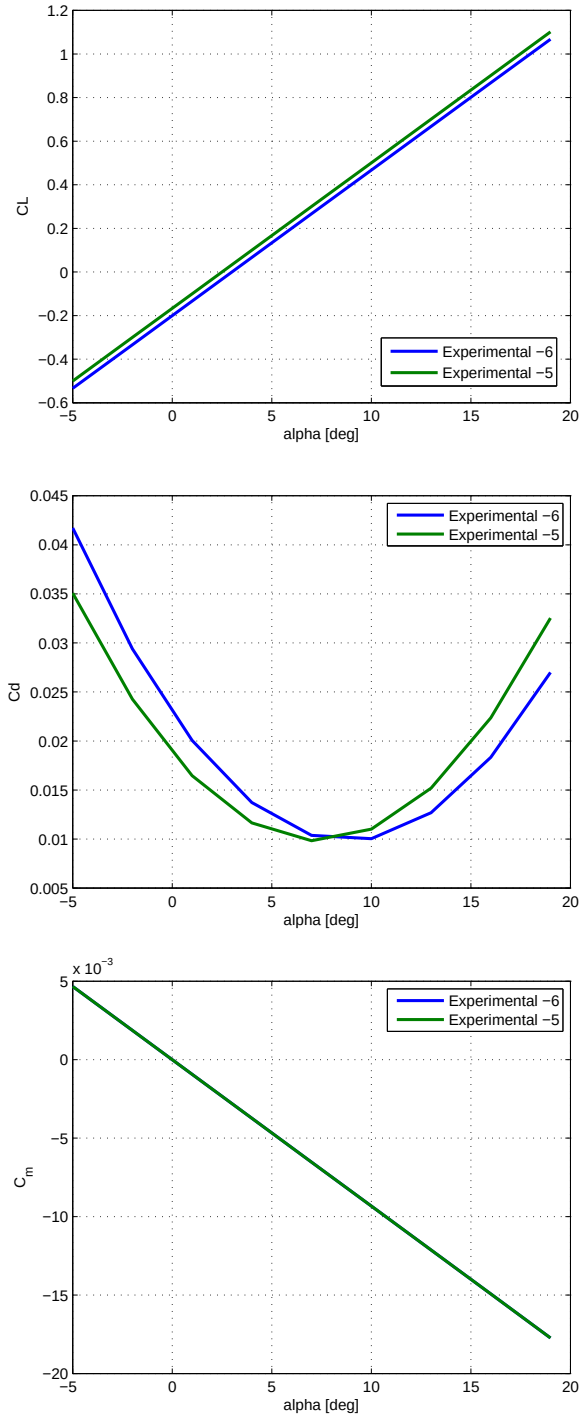

Figure 8.5: Uncoupled system lift curve slope (top), drag coefficient versus angle of attack (middle), and pitching moment coefficient versus angle of attack (bottom).

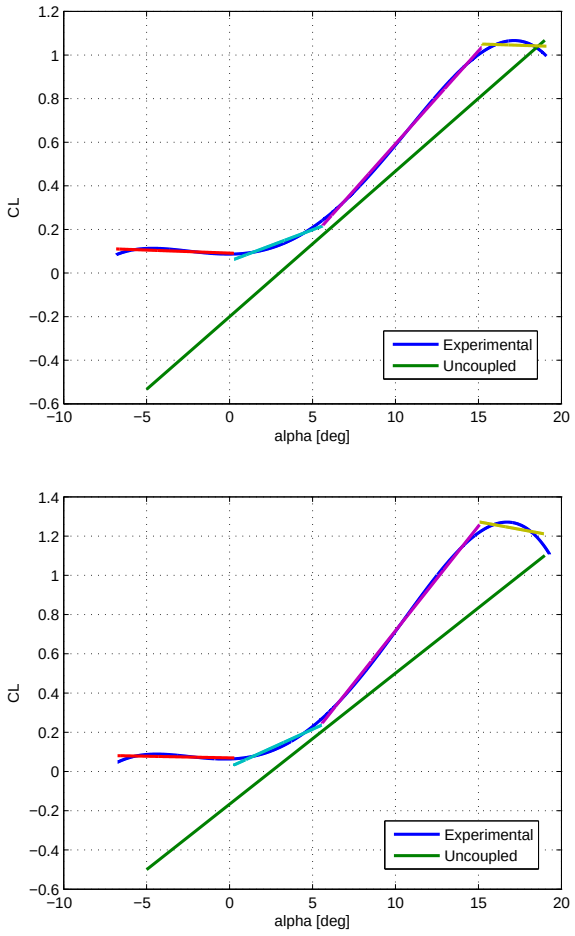

Figure 8.6: Experimental versus uncoupled system lift curve slope at $De = -5°$ (top), and $De = -6°$ (bottom).

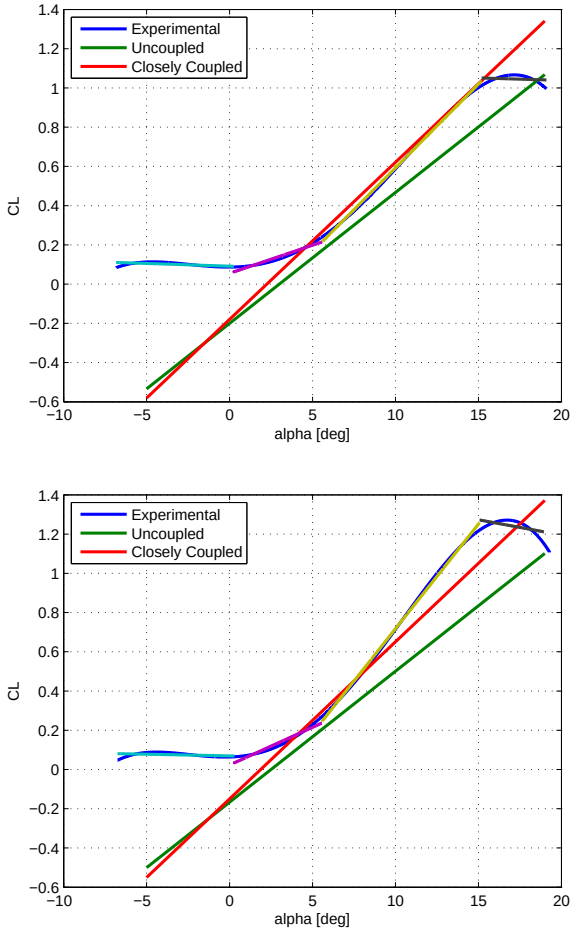

Figure 8.7: Experimental versus closely-coupled system, versus uncoupled system lift curve slope at $De = -5°$ (top), and $De = -6°$ (bottom).

Part V

Conclusions

Figure 8.8: Viking Dragonfly, ready to taxi.

What Has Been Achieved

The objective set at the beginning of this paper was to describe the tandem configuration as thoroughly as possible, through the definition of its design variants, the portrayal of its historical projects and engineering achievements, and the presentation of a simple mathematical model used to simulate the flight mechanics of this non conventional design. Another objective, which was not fully emphasised, was that to aid the reader in understanding just how difficult but yet intriguing the design of an aircraft in tandem configuration (or its derivatives) is.

While the historical description of the configuration, could be defined as ultimate and comprehensive, the mathematical model could be thought of as a starting point for a more developed and complex project, as it has not managed to fully reach its goal.

Future Development

The idea of having a disturbance model described by more than just (α, δ) could be further investigated both by mathematical trials and even through a remake of Olson's and Selberg's experiment. Copying the model biplane used, its configurations, test parameters needed, but varying the trials carried out, in order to properly investigate the downwash-decalage correlation, and support any other development of the mathematical model, if needed.

Bibliography

[1] Scharpr D.F. and Muellert T.J., "An Experimental Study of a Closely Coupled Tandem Wing Configuration at Low Reynolds Numbers", American Institute of Aeronautics and Astronautics, Inc., 1990.

[2] Rutan B., "Quickie-Type Aircraft Design Origins", EAA Sport Aviation, October 1981.

[3] Tobin J., "To Conquer The Air: The Wright Brothers and the Great Race for Flight", Free Press division of Simon & Schuster, Inc. 2003.

[4] Col. Butler G., "That Other Air Service Centennial", Naval History, June 2012, p. 54.

[5] Goetz A., "Pitt Magazine", University of Pittsburgh Office of Public Affairs. Fall 2007; pp. 3.

[6] Jakab P.L., "The Original", Air&Space/Smithsonian, March 2003, pp. 34–39.

[7] Mikesh R.C. and Tom D.C., "Restoration: The Wright Flyer", National Air and Space Museum Research Report, 1985, pp. 135–141.

[8] Jane F. T., "Jane's All the World's Aircraft 1913", Newton Abbot, UK, David & Charles, 1969.

[9] Davilla J.M. and Arthur M.S., "French Aircraft of the First World War", Flying Machines Press, Stratfort, Connecticut, 1997.

[10] Ord-Hume A.W.J.G, "Flying Flea, Henri Mignet's Pout-du-Ciel", Catrine, Stenlake Publishing, 2011.

[11] Bowers P.M., "Guide to Homebuilts - Ninth Edition", TAB Books, 1984.

[12] Crouch T.D., "Blériot XI: The Story of a Classic Aircraft", Washington, D.C., Smithsonian Institution Press, 1982.

[13] Green W., "War Planes of the Second World War: Volume One Fighters", London, Macdonald, 1967.

[14] Green W., "War Planes of the Second World War: Volume Three Fighters", London, Macdonald, 1967.

[15] Dale V., "Ш-Тандем" [Sh-Tandem], Ugolok neba, 2013.

[16] Gordon Y. and Komissarov D., "OKB Mikoyan: A History of the Design Bureau and its Aircraft", Hinckley, England, Midland Publishing, 2009.

[17] Thompson J.W., "Italian Civil and Military aircraft 1930-1945", New York: Aero Publishers Inc. pp. 17–18.

[18] Tiberi L., "Ali Italiane: Storie di uomini e di macchine volanti" [Documentary], Istituto Luce, 2005.

[19] Balzer G.H, "American Secret Pusher Fighters of World War II: XP-54, XP-55, and XP-56", North Branch, Minnesota, Specialty Press, 2008.

[20] Grey C.G., "Jane's All the World's Aircraft 1938", London, David & Charles, 1972.

[21] Dyer E.M. III, "Japanese Secret Projects:Experimental aircraft of the IJA and IJN 1939-1945" (1st ed.), Hersham, Ian Allan Publishing, 2009, pp. 104–106.

[22] Buttler T., "British Secret Projects Fighters & Bombers, 1935-1950", Hinckley, Midland Publications, 2004.

[23] Rokhsaz K. and Selberg B.P.,"Dual-Wing Systems with Decalage Angle Optimization", Journal of Aircraft, Vol. 23 No. 5, May 1986.

[24] Molina G.J., Garcia J.O, Fuentes J.N., Herrera D.A., "A study of lift for a tandem-biplane wing configuration: screening of geometric factors by computer simulation", Proceedings of the XIth International Congress and Exposition, Orlando, Florida USA, 2008.

[25] Fanjoy D.W., Dorney D.J., "Numerical Simulations of Tandem-Airfoil Aerodynamics", Aerospace Atlantic Conference, SAE Int., Ohio, USA, May 1996.

[26] Broering T.M. and Yongsheng Lian, "The Effect of Wing Spacing on Tandem Wing Aerodynamics", AIAA Applied Aerodynamics Conference, Chicago, Illinois, USA, June-July 2010.

[27] Olson E.C. and Selberg B.P., "Experimental Determination of Improved Aerodynamic Characteristics Utilizing Biplane Wing Configurations", Journal of Aircraft, Vol. 13 No. 4, April 1976.

[28] LI Feng, YE ZhengYin and GAO Chao, "Design of a New Tandem Wings Hybrid Airship", National Key Laboratory of Aerodynamic Design and Research, Northwestern Polytechnical University, China, 2012.

[29] Laitone E.V., "Prandtl's Biplane Theory Applied to Canard and Tandem Aircraft", Journal of Aircraft, Vol. 17 No. 4, April 1980.

[30] Kendall E.R., "The Minimum Induced Drag, Longitudinal Trim and Static Longitudinal Stabiliity of Two-Surface and Three-Surface Airplanes", 2nd Applied Aerodynamics Conference, Seattle, Washington, USA, August 1984.

[31] Wolkovitch J., "Subsonic VSTOL Aircraft Configurations with Tandem Wings", Journal of Aircraft, Vol. 16 No. 9, September 1979

[32] Rokhsaz K., "Analytical Investigation of the Aerodynamics Characteristics of Dual Wing Systems", University of Missouri, Rolla, 1980.

[33] Somnay, Rajesh J. "Design of Dual Wing Structures", UMR Thesis, Rolla, Mo., 1983.

[34] Abbott, Ira H. and Von Doenhoff, Albert E. "Theory of Wing Sections", Dover Publications , 1959.

[35] Holst T.L., "Viscous Transonic Airfoil Workshop Compendium of Results", AIAA Paper 87-1460, Honolulu, HI, 1987.

[36] Henshaw W.D. and Schwendeman D.W., "Moving Overlapping Grids with Adaptive Mesh Refinement for High-Speed Reactive and Non-reactive Flow," Journal of Computational Physics, Vol. 216, pp. 744-779, 2006.

[37] Rebuffet P., "Aerodinamique Experimentale", Librairie polytechnique CH. Beranger, Paris, France, 1966.

[38] Roskam J., "Airplane Design: Part I-VIII", DARcorporation, Lawrence, Kansas, 2002.

[39] Raymer D.P., "Aircraft Design-A Conceptual Approach", AIAA Education Series, 1999.

[40] Kuethe, Arnold M. and Chow, Chuen-Yen "Foundations of Aerodynamics: Basis of Aerodynamic Design", John Wiley & Sons, 1976..

[41] "The Distribution of Loads Between the Wings of a Biplane Having Decalage", NACA technical report No.269, p.18, November 1927.